ELSEVIER

Predicting the optical properties of the West Florida Shelf: resolving the potential impacts of a terrestrial boundary condition on the distribution of colored dissolved and particulate matter

W. Paul Bissett[a],[*], Robert Arnone[b], Sharon DeBra[a], Dwight A. Dieterle[c], Daniel Dye[a], Gary J. Kirkpatrick[d], Oscar M. Schofield[e], Gabriel A. Vargo[c]

[a]*Florida Environmental Research, 4807 Bayshore Blvd., Suite 101, Tampa, FL 3361, USA*
[b]*Code 7330, Naval Research Laboratory, Stennis Space Center, MS, USA*
[c]*College of Marine Science, University of South Florida, St. Petersburg, FL, USA*
[d]*Mote Marine Laboratory, Sarasota, Florida USA*
[e]*Institute of Marine and Coastal Science, Rutgers University, New Brunswick, NJ, USA*

Abstract

Predicting the distribution of Inherent Optical Properties (IOPs) in the water column requires predicting the physical, chemical, biological, and optical interactions in a common framework that facilitates feedback responses. This work focuses on the development of ecological and optical interaction equations embedded in a 2D hindcast model of the shallow water optical properties on the West Florida Shelf (WFS) during late summer/fall of 1998. This 2D simulation of the WFS includes one case with a Loop Current intrusion above the 40-m isobath and one with the Loop Current intrusion in addition to a periodic terrestrial nutrient supply below the 10-m isobath. The ecological and optical interaction equations are an expansion of a previously developed model for open ocean conditions (Bissett, W.P., Carder, K.L., Walsh, J.J., Dieterle, D.A., 1999a. Carbon cycling in the upper waters of the Sargasso Sea: II. Numerical simulation of apparent and inherent optical properties. Deep-Sea Research, Part I: Oceanographic Research Papers, 46 (2), 271–317; Bissett, W.P., Walsh, J.J., Dieterle, D.A., Carder, K.L., 1999b. Carbon cycling in the upperwaters of the Sargasso Sea: I. Numerical simulation of differential carbon and nitrogen fluxes. Deep-Sea Research, Part I: Oceanographic Research Papers, 46 (2), 205–269). The expansion includes an increase in the number of elemental pools to include silica, phosphorus, and iron, an increase in the number of phytoplankton functional groups, and a redevelopment of the Dissolved Organic Matter (DOM) and Colored Dissolved Organic Matter (CDOM) interaction equations. It was determined from this simulation that while the Loop Current alone was able to predict the water column conditions present during the summer, the Loop Current alone was not enough to simulate the magnitude of optical constituents present in the fall of 1998 when compared to satellite imagery. Simulating terrestrial inorganic and organic nutrients and CDOM pulses coinciding with significant

---

* Corresponding author. Tel.: +1 813 837 3374x102; fax: +1 813 902 9758.
 E-mail address: pbissett@flenvironmental.org (W.P. Bissett).

REPORT DOCUMENTATION PAGE				*Form Approved* OMB No. 0704-0188
The public reporting burden for this collection of information is estimated to average 1 hour per response, including the time for reviewing instructions, searching existing data sources, gathering and maintaining the data needed, and completing and reviewing the collection of information. Send comments regarding this burden estimate or any other aspect of this collection of information, including suggestions for reducing the burden, to the Department of Defense, Executive Services and Communications Directorate (0704-0188). Respondents should be aware that notwithstanding any other provision of law, no person shall be subject to any penalty for failing to comply with a collection of information if it does not display a currently valid OMB control number. **PLEASE DO NOT RETURN YOUR FORM TO THE ABOVE ORGANIZATION.**				

1. REPORT DATE *(DD-MM-YYYY)* 22-09-2004	2. REPORT TYPE Journal Article (refereed)		3. DATES COVERED *(From - To)*	
4. TITLE AND SUBTITLE Predicting the optical properties of the West Florida Shelf: resolving the potential impacts of a terrestrial boundary condition on the distribution of colored dissolved and particulate matter		**5a. CONTRACT NUMBER**		
		5b. GRANT NUMBER		
		5c. PROGRAM ELEMENT NUMBER PE0601153N		
6. AUTHOR(S) Bissett, Paul W., Arnone, Robert, DeBra, Sharon, Dieterle, Dwight A., Dye, Daniel, Kirkpatrick, Gary J., Schofield, Oscar M.,Vargo, Gabriel A.		**5d. PROJECT NUMBER**		
		5e. TASK NUMBER		
		5f. WORK UNIT NUMBER 73-8028-B3-5		
7. PERFORMING ORGANIZATION NAME(S) AND ADDRESS(ES) Naval Research Laboratory Oceanography Division Stennis Space Center, MS 39529-5004		**8. PERFORMING ORGANIZATION REPORT NUMBER** NRL/JA/7330-03-10		
9. SPONSORING/MONITORING AGENCY NAME(S) AND ADDRESS(ES) Office of Naval Research 800 N. Quincy St. Arlington, VA 22217-5660		**10. SPONSOR/MONITOR'S ACRONYM(S)** ONR		
		11. SPONSOR/MONITOR'S REPORT NUMBER(S)		

12. DISTRIBUTION/AVAILABILITY STATEMENT

Approved for public release, distribution is unlimited.

13. SUPPLEMENTARY NOTES * U.S Government Author : Arnone

14. ABSTRACT

This work focuses on the development of ecological and optical interaction equations embedded in a 2D hindcast model of the shallow water optical properties on the West Florida Shelf (WFS) during late summer/fall of 1998. This 2D simulation of the WFS includes one case with a Loop Current intrusion above the 40-m isobath and one with the Loop Current intrusion in addition to a periodic terrestrial nutrient supply below the 10-m isobath. The ecological and optical interaction equations are an expansion of a previously developed model for open ocean conditions.

It was determined from this simulation that while the Loop Current alone was able to predict the water column conditions present during the summer, the Loop Current alone was not enough to simulate the magnitude of optical constituents present in the fall of 1998 when compared to satellite imagery.

15. SUBJECT TERMS

Inherent optical properties; CDOM; Ecological modeling; Terrestrial nutrients; Non-Redfeld ratios; Biogeochemical processes; USA; Florida; Gulf of Mexico; West Florida Shelf

16. SECURITY CLASSIFICATION OF:			17. LIMITATION OF ABSTRACT	18. NUMBER OF PAGES	19a. NAME OF RESPONSIBLE PERSON Robert Arnone
a. REPORT	b. ABSTRACT	c. THIS PAGE	UL	35	
Unclassified	Unclassified	Unclassified			19b. TELEPHONE NUMBER *(Include area code)* (228) 688-5268

Standard Form 298 (Rev. 8/98)
Prescribed by ANSI Std. Z39.18

PUBLICATION OR PRESENTATION RELEASE REQUEST

Pubkey: 3618

NRLINST 5600.2

1. REFERENCES AND ENCLOSURES

Ref: (a) NRL Instruction 5600.2
(b) NRL Instruction 5510.40D

Encl: (1) Two copies of subject paper
(or abstract)

2. TYPE OF PUBLICATION OR PRESENTATION

( ) Abstract only, published
( ) Book
( ) Conference Proceedings
(refereed)
( ) Invited speaker
(X) Journal article (refereed)
( ) Oral Presentation, published
( ) Other, explain

( ) Abstract only, not published
( ) Book chapter
( ) Conference Proceedings
(not refereed)
( ) Multimedia report
( ) Journal article (not refereed)
( ) Oral Presentation, not published

3. ADMINISTRATIVE INFORMATION

STRN NRL/JA/7330-03-10
Route Sheet No. 7330/
Job Order No. 73-8028-B3-5
Classification __X__ U ____ C
Sponsor ONR BASE
approval obtained __X__ yes ____ no

4. AUTHOR

Title of Paper or Presentation

Predicting the Optical Properties of the West Florida Shelf: Resolving the Potential Impacts of a Terrestrial Boundary Condition on the Distribution of Colored Dissolved and Particulate Matter

Author(s) Name(s) (First,MI,Last), Code, Affiliation if not NRL

Paul Bissett, Robert A Arnone, Sharon DeBra, Dwight Dieterle, Daniel Dye, Gary Kirkpatrick, Oscar Schofield, Gabriel Vargo, John Walsh

It is intended to offer this paper to the _____
(Name of Conference)

_____
(Date, Place and Classification of Conference)

and/or for publication in **Marine Chemistry, Unclassified**
(Name and Classification of Publication)   (Name of Publisher)

After presentation or publication, pertinent publication/presentation data will be entered in the publications data base, in accordance with reference (a).
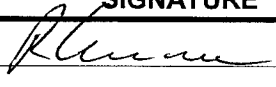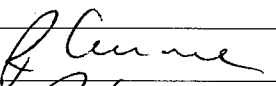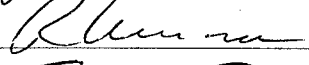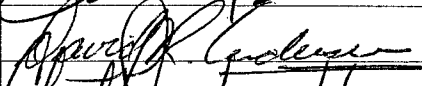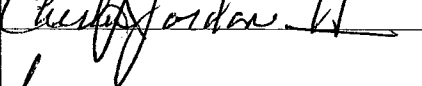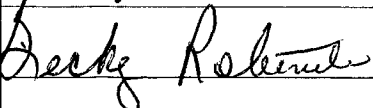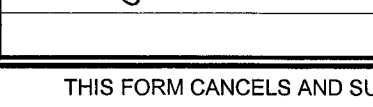It is the opinion of the author that the subject paper (is _____) (is not __X__) classified, in accordance with reference (b).
This paper does not violate any disclosure of trade secrets or suggestions of outside individuals or concerns which have been communicated to the Laboratory in confidence. This paper (does _____) (does not __X__) contain any militarily critical technology.
This subject paper (has _____) (has never __X__) been incorporated in an official NRL Report.

_____
Robert A Arnone, 7333
Name and Code (Principal Author)

_____
(Signature)

5. ROUTING/APPROVAL

CODE	SIGNATURE	DATE	COMMENTS
Author(s) Arnone	*[signature]*		
Section Head N/A	*[signature]*		
Branch Head Arnone	*[signature]*	4/1/03	
Division Head Payne, acting	*[signature]*	4/1/03	1. Release of this paper is approved. 2. To the best knowledge of this Division, the subject matter of this paper (has _____) (has never __X__) been classified.
Security, Code 7030.1	*[signature]*	4/4/03	1. Paper or abstract was released. 2. A copy is filed in this office. SSC-130-3
Office of Counsel,Code 1008.3	*[signature]* Chris Jordan II	4/18/03	
ADOR/Director NCST E.O. Hartwig, 7000	*[signature]*		
Public Affairs (Unclassified/ Unlimited Only), Code 7030.4	*[signature]*	4/9/03	Add acknowledgments
Division, Code			
Author, Code			

HQ-NRL 5511/6 (Rev. 12-98) (e)   THIS FORM CANCELS AND SUPERSEDES ALL PREVIOUS VERSIONS

meteorological events and high freshwater pulses released from the major rivers feeding the WFS were required to accurately predict the distribution and scale of the inherent optical properties at the surface during the fall months. Modeling the in situ light field for phytoplankton growth and community competition requires addressing the CDOM optical constituent explicitly. The majority of the annually modeled CDOM on WFS was created via in situ production; however, it was also rapidly removed via advection and photochemical destruction. A pulse of terrestrial nutrient and organic color was required to simulate the dramatic changes in surface color seen in satellite imagery on the WFS. The dynamics of the biogeochemical portion of the simulation demonstrate the importance of nonstoichiometric supplies of terrestrial nutrients on the WFS to the prediction of nutrient and CDOM fluxes.

1. Introduction

The color and clarity of the water column is directly attributed to the depth-dependent distribution of the mass of particulate and dissolved matter and its associated optical properties, i.e., the inherent optical properties (IOPs) of the water column. The biochemical mass in the water column can be broken down into constituent parts of living organic (viruses, bacterioplankton, phytoplankton, zooplankton, fish, mammals, etc.), nonliving organic [Dissolved Organic Matter (DOM), detritus, marine snow, etc.], nonliving inorganic (elements, salts, and sediment), and water itself. Of these mass constituents, the sum of bacterioplankton, phytoplankton, DOM, detritus, marine snow, sediments, and the water itself composes the greatest impact on water column color and clarity (Gordon et al., 1983; Mobley and Stramski, 1997; Stramski and Mobley, 1997). Each of these constituents has a unique optical signature, defined by its IOPs of absorption, scattering, and scattering phase function. It is the uniqueness of these constituent signatures that has given rise to the ability of inverting a color signal, e.g., satellite ocean color remote sensing, into estimates of pigments, as an estimate of phytoplankton biomass, and colored DOM as a proxy for fresh water releases to the coastal ocean.

The inversion of an ocean color signal into the optical constituents of phytoplankton, Colored Dissolved Organic Matter (CDOM), and sediments is far less time consuming than estimating their spatial and temporal distribution with ship surveys. However, the remote sensing estimate may be less accurate than simultaneously collected survey data, in part because of the algorithms that relate water-leaving radiance to optical constituents. These algorithms use assumptions about constituent optical properties and vertical structure that may not accurately describe a given individual in situ sample. Yet, ocean color remote sensing may offer a better means of estimating optical constituents at locations and times that are not covered by surveys (e.g., Del Castillo et al., 2001; Toole and Siegel, 2001; Yoder et al., 2002). In particular, the time and space interpolation between in situ samples often masks the true variance in the distribution of phytoplankton and CDOM. Thus, measuring the water-leaving radiance may offer the potential to sample the ecological state of the water column at higher temporal and spatial frequencies than traditional in situ sampling.

Modeling efforts to forecast or hindcast the ecological state of the water column, and the concomitant mass constituents, often use satellite-derived chlorophyll a estimates as a means of validating their solutions (e.g., Bissett et al., 1994; Gregg and Walsh, 1992; Walsh et al., 1989, 1999, 2002). These modeling efforts use a series of linked physical, chemical, and biological equations to approximate the myriad of ecological interactions that exist in the ocean. The models differ in many respects but are all fundamentally the same in that the mass of phytoplankton is a function of the growth and mortality processes (Riley, 1946), and that the growth processes are a function of the available light and nutrients. The main differences between these ecological models are in the complexity of their interaction equations and number of mass constituents

(state variables). At the simplest level, there are the single limiting resource Phytoplankton–Zooplankton–Nutrient (PZN) models (e.g., Wroblewski, 1977). At the other end of the modeling spectrum exist models that solve for multiple limiting nutrients with non-stoichiometric interactions (Bissett et al., 1999a,b; Moore et al., 2001).

Validation of these ecological models can be difficult, particularly because the solutions are directly related to the physical circulation, which itself is difficult to simulate. The validation of ecological models by in situ surveys is difficult because of the limitations and aliasing difficulties presented by large-scale surveys. Validation of these models by remote sensing may be the only means to adequately resolve the temporal and spatial frequencies that are predicted by the models.

Confirmation of ecological models using satellite-derived proxies for biomass (e.g., chlorophyll) often suffers from many of the same assumptions and problems associated with validation by in situ comparisons. The most commonly used satellite algorithms often assume (1) a fixed vertical structure and (2) a constant relationship between biomass and chlorophyll. There are some variations on the chlorophyll to biomass relationship (e.g., Carder et al., 1999), which attempt using other variables such as temperature as a means of establishing optimal biomass to chlorophyll a relationships by virtue of altering the estimated "packaging" effects. However, the real limitation with this validation approach is that a satellite-derived property (which is estimated using an algorithm with its own possible difficulties) is being used to validate an ecological simulation with other, frequently different, assumptions.

For modeling efforts to realistically portray the marine environment, feedback between the physical, chemical, biological, and optical forcing functions must be explicitly incorporated (Bissett et al., 2001). Most ecological simulations assume a constant relationship between a proxy for phytoplankton biomass, i.e., chlorophyll, and the light and nutrient interactions that drive phytoplankton growth. This static solution is problematic when multiple functional groups of phytoplankton are responsible for the biogeochemical alteration of nutrient and carbon stocks. Coastal waters are particularly difficult to

model with this approach. One approach to resolving the complex interactions between light, nutrients, and phytoplankton growth is to explicitly resolve the feedback of these interactions on the Inherent Optical Properties (IOPs) of the water column (Bissett et al., 1999a,b).

By coupling these interactions explicitly, one may also simultaneously use the light field as well as the time-dependent change of measurable optical properties, such as total absorption and scattering, as validation data. The light field may be measured directly in situ with upwelling and downwelling radiometers as well as via remote sensing. The effort to develop a predictive optical/ecological simulation starts with the prediction of the IOPs of absorption, scattering, and scattering phase function as characteristics of the mass constituents of the water column. This work focuses on developing predictive IOP simulations starting with an attempt to hindcast the West Florida Shelf (WFS) during the fall of 1998. Two companion papers will follow evaluating additional modeled output data and expanding upon results from the model runs presented here; one will focus on the prediction of algal species (Bissett et al., 2003) and the second will focus on the validation of the simulated radiance results against observed satellite radiances (Bissett et al., 2004a).

2. Ecological background of the West Florida Shelf

For the most part, the WFS is an oligotrophic shelf region, with the episodic occurrences of high levels of color resulting from nutrient and organic additions to the shelf. These episodic occurrences result mainly from three types of ecological events: (1) discharges from fresh water systems that have high concentrations of nutrients and organic matter (Del Castillo and Coble, 2000; Del Castillo et al., 2000; Dragovich et al., 1968; Gilbes et al., 1996; Kim and Martin, 1974); (2) the Loop Current via episodic upwelling on "the left borders of currents" (Bogdanov et al., 1967) caused by western boundary currents (Pond and Pickard, 1989; Tester and Steidinger, 1997); and (3) organic nitrogen injection resulting from aeolian supplies of iron to nitrogen-fixing cyanobacteria (Lenes et al., 2001; Walsh and Steidinger, 2001).

The paradox of the WFS is that it has been the site of toxic concentrations of *Karenia brevis* (*K. brevis*, formerly *Gymnodinium breve* Davis; $>1 \times 10^4$ cells l^{-1}) for 42 of the last 49 years (Florida Fish and Wildlife Conservation Commission and Florida Marine Research Institute (FMRI); Steidinger, 2003; per comm.), and that these Harmful Algal Blooms (HABs) occur in traditionally optically clear, nutrient-poor waters. The importance of these episodic events can be seen in the optical data as the extreme change in the IOPs from Jerlov-type I–III (i.e., optically clear) waters typically found in the Gulf of Mexico (Bissett et al., 1997) to those resulting from *K. brevis* bloom conditions of >60 µg chl a l^{-1} (Carder and Steward, 1985) with phytoplankton absorption, $a_p(440)$, and CDOM absorption, $a_g(440)$, values of 0.2 and ~0.2 m^{-1}, respectively. These values are an order of magnitude greater than background values on the WFS (Del Castillo et al., 2000).

Prediction of these IOP events will require a systematic understanding and quantification of physical, chemical, biological, and optical interactions. In 1998, as part of a joint Office of Naval Research (ONR)/Naval Research Laboratory (NRL)/National Oceanographic and Atmospheric Administration (NOAA)/Environmental Protection Agency (EPA) and State of Florida funded project–Ecology of Harmful Algal Blooms-Florida (ECOHAB-Florida, NOAA, EPA, ONR), Spectral Signatures of the Littoral Zone (NRL), and the Coastal Ocean Monitoring and Prediction System (COMPS, State of Florida) studies, a series of experiments were conducted to study phytoplankton ecology and the biooptical properties of the West Florida Shelf (Fig. 1). The program on the WFS had two distinct field components. The first component was a hydrographical description of the monthly water characteristics. This first component had two parts: part A
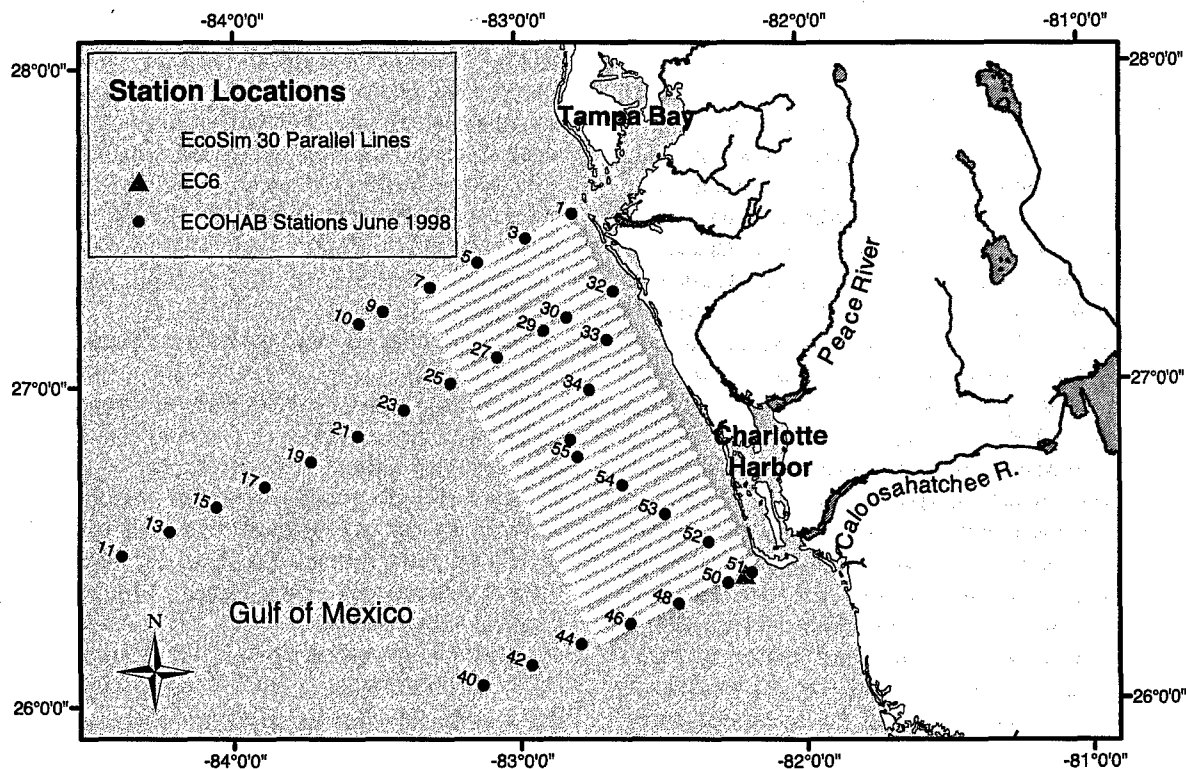
Fig. 1. Location of ECOHAB nutrient stations on the WFS during June 1998 with corresponding station location numbers. The lines perpendicular to the coast are the "EcoSim 30 parallel lines" extending from the 10-m isobath to approximately 60 km from the 10-m isobath ("entire domain"). Note—this region is smaller across the shelf than the box enclosed by the ECOHAB monthly cruises. Lines are numbered 1 to 30 from Tampa Bay to Charlotte Harbor. Location of bottom-mounted mooring EC6 (depth of 10 m) adjacent to Charlotte Harbor.

consisted of two sets of monthly hydrological survey cruises conducted between Tampa Bay and Charlotte Harbor (Florida Fish and Wildlife Conservation Commission and Florida Marine Research Institute–ECOHAB Cruise Data, 2004) and part B consisted of Acoustic Doppler Current Profiler (ADCP) moorings and meteorological buoys operating continuously during the year (University of South Florida Coastal Ocean Monitoring and Prediction System, 2004). The second component of the experiment occurred during October/November of that year. This experiment was a process study designed to hunt for *K. brevis* populations via ship, satellite, aircraft, and mooring data streams and attempt to quantify the ecology of these populations (Mote Marine Laboratory ECOHAB Cruise Flow Through Surface Maps, 2004). These experiments were conducted by Florida Department of Environmental Protection (DEP), University of South Florida (USF), NRL, University of Southern Mississippi (USM), Mote Marine Laboratory (MML), and Florida Environmental Research Institute (FERI).

Our initial development of this optical/ecological simulation in coastal waters focuses on the WFS during 1998, as this year contained both a large Loop Current intrusion in the summer and heavy fresh water flows from the Charlotte Harbor estuary following the passages of Hurricanes Georges and Mitch in the fall. In order to test these two potential episodic event mechanisms on IOP formation, we develop here a 2D physical simulation that includes both Loop Current intrusions above the 40-m isobath and episodic pulses of fresh water below the 10-m isobath by utilizing CDOM as a tracer for terrestrial inputs. We will use this 2D physical forcing to drive an ecological/optical simulation that allows for non-stoichiometric supply and uptake of nutrients, and spectral light harvesting by the autotrophic community to effect phytoplankton competition as well as the allocthonous supply and autocthonous creation and destruction of CDOM.

Our goal in this initial paper is to describe a set of ecological interaction equations that incorporate optics as a fundamental component of its structure. As this is a model of the coastal zone, this model must include terrestrial boundary conditions in a consistent manner that preserves its numerical stabilities while providing results that are directly comparable to the available validation data streams. The goal in this effort is to specifically avoid reductionism, which would provide only a minimal set of interaction equations that specifically describe this site and data set. This effort is focused on a more broad set of ecological equations, which may be applied to multiple environments, with minimal parameter tuning, such that its application may be robust across multiple ecotones (transitional zones between two communities containing the characteristic species of each). This approach will allow for a single ecological model to be used for multiple coastal regimes within the same simulation experiment.

3. Methodology

This numerical study expands upon the framework of a previously developed open ocean ecological model, EcoSim (Bissett et al., 1999a,b). That model was driven by seasonal changes in spectral light, temperature, and water column mixing. The previous model was modified to generate a coastal ocean ecological simulation examining the ecological and optical properties on the West Florida Shelf. The key highlights of this expanded model are (1) nonstoichiometric elemental cycling through (2) multiple functional groups of phytoplankton, which are described by (3) explicit descriptions of their spectral inherent optical properties that are (4) allowed to change as a function of cellular light and nutrient exposure. In addition, the model includes (5) explicit descriptions of multiple classes of dissolved organic matter and colored dissolved organic matter as well as their spectral inherent optical properties. The explicit inclusion of spectral inherent optical properties (IOPs) allows for a more robust description of the available light field for ecological cycling of elements as well as to provide additional simulated data by which to substantiate the model. The model (referred to as EcoSim) has been expanded for this coastal application to include seven functional groups of phytoplankton. Other major changes include the expansion of the number of elements from two (carbon and nitrogen) to five (carbon, nitrogen, silica, phosphorus, and iron). The model is described mathematically in a separate technical document due to space limitations (Bissett et al., 2004b).

3.1. Dissolved organic matter

This paper seeks to use color as a validation data set for the sum total of ecological cycling on the WFS. In the coastal zone, color is frequently dominated by the dissolved organic pool, and this effort seeks to describe the cycling of this organic pool as part of a larger ecological and optical effort. DOM can be thought of as a temporary storage pool for the cycling of elements between inorganic and particulate organic phases. The residence time of the elements in this pool can be >1000s of years (Williams and Druffel, 1987), months to years (Carlson, 2002), or <1 day (Carlson and Ducklow, 1996; Carlson et al., 1996). Part of the problem in attempting to address this pool is that it undergoes constant biological and chemical trans-formations, resulting from heterotrophic and photo-chemical processes that strip easily accessible energy and elements from freshly produced DOM. This results in a pool of material that is amorphous, with little physical description from the field other than total elemental quantities of material that pass through a 0.2-μm filter (Carlson, 2002).

There are a few things that are definitively known about the cycling of DOM. First, bacteria use DOM as an energy source, regenerating inorganic carbon, nitrogen, and phosphorus in the process (Banse, 1995; Carlson and Ducklow, 1996; Goldman et al., 1987; Kirchman et al., 1989, 1990). Second, as labile energy and elements are removed, the residence time of the remaining material gets longer. Third, ele-mental forms of nitrogen and phosphorus can be taken from DOM by bacteria and phytoplankton without measurable transition through inorganic phases, e.g., phosphorus-based growth without meas-urable increases in DIP (Mulholland et al., 2002). Fourth, older, biologically refractory DOM typically has a lower fraction of nitrogen and phosphorus per unit carbon than does DOM produced from primary production, suggesting that the nutrients of nitrogen and phosphorus are preferentially removed during the biological transformation of DOM (Clark et al., 1998).

DOM is modeled in this simulation with these known attributes by using two forms of DOM, a semilabile form that represents material with turnover times on order of days to weeks (the average residence time of this semilabile pool given the parameters selected for this simulation is approximately 44 days) and a relict form with turnover times greater than the length of our simulation (>10s of years; Hansell and Carlson, 2002). All primary and secondary produced DOM in the model pass through the labile pool. The relict pool is created during bacteria reprocessing of the labile pool. The relict form is analogous to a permanent sink of elements from our model. The exception to this permanent sink rule is that the colored component of the relict DOM pool can be photochemically transformed from the relict CDOM pool and placed into the inorganic pools and labile DOM pool.

In coastal environments that receive terrestrial runoff, a significant fraction of the total terrestrial supply of bioavailable nutrients may be in DOM form. To address the issues of variations in the time-dependent ratios of elemental composition in the DOM pool, the elements of carbon, nitrogen, and phosphorus are carried as independent state variables in both the labile and relict pools (there is no assumed pool of dissolved organic silica or iron).

An added complexity about DOM is that some fractions of the molecular bonds within the amor-phous organic pool are light absorbing. On the WFS, CDOM is a major component (Carder et al., 1989; Del Castillo et al., 2000; Gilbes et al., 1996; Steward et al., 1978) to the attenuation of light in the water column. Modeling the in situ light field for phytoplankton growth and community competition requires address-ing this optical constituent explicitly. There is often a delineation in the study of DOM between total DOM and CDOM as the pools appear to be coupled but not necessarily tightly (Del Castillo et al., 2000; Rochell-Newall et al., 1999). The sources and sinks of DOM and CDOM are coupled through the processes of formation, photolysis, photooxidation, and heterotro-phic use; however, there is no simple linear trans-formation function that can be used to relate one to the other (Vodacek et al., 1997). Using laboratory studies on the cycling of CDOM and DOM (e.g., Miller and Zepp, 1995; Moran et al., 2000), the chromophoric pool of DOM can be described as a separate state variable tied to the cycling of DOM. The added advantage of directly modeling CDOM is that it provides an additional validation data set for the physical model as well as the ecological model because there is a nearly linear relationship between

salinity and CDOM absorption near the terrestrial outflow areas (e.g., Del Castillo et al., 2000). While an exact relationship is dependent upon the drainage area, the linearity is driven by the fact that the process of physical mixing occurs at rates that are greater than the rate of formation and destruction.

As an aside, in this model, there are two forms of colored degradational material, colored dissolved organic carbon ($CDOC_1$) and $CDOC_2$. These are tracked as state variables, which are in total called colored degradational material (CDM). It is assumed here that the carbon associated with this color pool may act as a good proxy for all of the degradational colored matter. There is some debate within the color community as to the veracity of this assumption. However, inverse methods for determining absorption from satellite-derived ocean color (e.g., Sea-WiFS) are not routinely capable of differentiating between CDOM and detrital absorption and therefore estimate the sum of all colored degradational material (Nelson et al., 1998; Siegel et al., 2002). In addition, field studies suggest that detrital particulate absorption constitutes only a small fraction of the total CDM absorption. For these reasons, the term CDM is used when referring to the combined simulation of $CDOC_1$ and $CDOC_2$ and may be compared against the total color associated with observed CDOM in this manuscript.

3.2. Optical properties

This paper uses optical properties and satellite-derived estimates of optical properties as its major source of validation data. Light may be considered similar to nutrients in that the ecological dynamics help determine the quantity and spectral quality of the downwelling photon density. The spectral photon density in turn drives positive and negative feedbacks within the individual components of the ecosystem. As mentioned above, light harvesting by phytoplankton is assumed to be a function of the available downwelling energy at depth. Since light energy is attenuated at different rates depending on the wavelength, the depth-dependent photosynthetically available radiation is spectrally variable. Here, photon density and harvesting were explicitly calculated at 5-nm intervals. This formulation allows for the differentiation of phytoplankton by the pigment suites and spectral photosynthetic efficiencies, providing competitive advantages to those species that can optimize light absorption and photochemical conversion at different depths and color zones.

In this model, an explicitly defined suite of IOPs was developed for each optical constituent in the model, i.e., phytoplankton, CDOM, detritus, etc. The time-dependent change in these mass constituents drove the associated modifications in the coupled IOPs. The IOPs were then used to calculate the Apparent Optical Properties (AOPs) of downwelling irradiance, $E_d(\lambda)$, with a numerically efficient single scattering approximation (Bissett et al., 1999a) as well as remote sensing reflectance, $R_{rs}(\lambda)$, with a more advanced radiative transfer model (Hydrolight 4.1, Mobley, 1994). These procedures allowed us to validate the biogeochemical simulation with in situ optical instruments, e.g., WetLabs AC-9, as well as spectral remote sensing products from multispectral satellite sensors, e.g., SEA-viewing Wide Field-of-view Sensor (SEAWiFS) and Moderate resolution Imaging Spectroradiometer (MODIS), and hyperspectral aircraft sensors, e.g., AVIRIS (Airborne Visible/InfraRed Imaging Spectrometer) and PHILLS (Portable Hyperspectral Imager for Low Light Spectroscopy).

A complete mathematical description of the model (EcoSim) is given in Bissett et al., 2004b. The simulation's organic and inorganic fields were initialized as described in Table B.1. The year-over-year change over all state variables was >0.1% after the first year, but the simulation was run for an additional 2 years to eliminate any numerical transients. Fluxes at the sea surface and the bottom were defined to be zero (details of the bottom boundary assumptions can be found in Bissett et al., 2004b). The fluxes at the shoreward boundary were set to zero, with the exception of the Charlotte Harbor pulse case where the impacts of a pulse were simulated on Day-Of-Year (DOY) 267 (September 24th) and 309 (November 5th; described below). The gulf-side boundary conditions change seasonally and were derived from the 1998/1999 ECOHAB cruises on the WFS (Fig. A.1). All the partial differential equations were solved explicitly with a forward-in-time, centered-in-space method (O'Brien, 1986).

The physical description of the 2D circulation fields were calculated as a response to surface winds and cross-shelf density gradients in the presence of bottom momentum stresses and horizontal diffusion. Advection of momentum is ignored, and the cross-shelf density gradient is a prescribed term independent of depth and the offshore coordinate. The formulation for the circulation submodel can be found in Appendix B. The flows were identical in the shoreward pulse and the nonpulse case.

3.3. Shoreward boundary conditions

It became evident in some of the early simulation analyses that an explicit inclusion of shoreward boundary conditions was required to predict the color on the WFS. In order to reproduce these required shoreward boundary conditions, nutrient data for the Charlotte Harbor region were collected and analyzed from the following agencies: Environmental Protection Agency's Office of Water Quality Storage and Retrieval (STORET) Database, Florida International University's Southeast Environmental Research Center, US Geological Survey (USGS) Water Quality for the Nation, US Army Corps of Engineers, Southwest Florida Water Management District, South Florida Water Management District, and The University of South Florida's ECOHAB Cruises. Data were collated in time and space and were placed in a geographical information system (GIS) database for retrieval.

The incorporation of shoreward boundary conditions is significant because terrestrial nutrient concentrations [Dissolved Organic Nitrogen (DON), Silica (SiO_2), Dissolved Organic Phosphorus (DOP), Nitrate (NO_3^-), and Orthophosphate ($o\text{-}PO_4$)] and color constituents (CDOM and sediments) were greater in rivers and estuaries flowing onto the WFS than the concentrations of these materials at the offshore boundary. The flux of nutrients at the boundary is paramount to the model solution. On the WFS, the stoichiometry of the boundary flux also provides critical habitat differences. In particular, the shoreward nitrogen and phosphorus fluxes were dominated by different forms and at different proportions than the offshore boundary conditions. At the shoreward boundary, it was determined that, in over 57% of the cases, total organic nitrogen was

the major contributor (>90%) to the TN concentration (in 95% of the cases, TON represented over 50% of the TN concentration). This finding demonstrates the significant contribution organic nitrogen makes to the concentration of TN and that its direct inclusion in any modeling effort is therefore crucial to precisely and accurately model the ecological dynamics of the WFS.

The relationship between TP and TOP was different, as $o\text{-}PO_4$ constituted a much larger proportion of TP. TOP was the major contributor (>90%) to the TP concentration in only 11% of the cases. It was still a significant fraction, as in 49.8% of the cases, TOP represented over 50% of the TP concentration. This is to be expected in this location, as elevated inorganic phosphate concentrations are a unique feature of the Peace River drainage basin, for this basin includes the Hawthorne Phosphatic Formation. Inorganic phosphate concentrations represented the majority (>50%) of the TP concentration in 50.2% of the samples (in 13% of the cases, $o\text{-}PO_4$ was the major contributor [>90%] to the TP concentration). These relationships between inorganic and organic supplies of phosphorus and nitrogen suggest that the inclusion of organic sources of nutrients (in particular nitrogen) as well as their relative stoichiometric supply relationships is a requirement to accurately simulate phytoplankton competition and assemblage speciation on the WFS.

In the fall of 1998, peaks in nutrient concentration correlated with peaks in discharges released from the Peace River (Fig. 2; image shown is of Total Nitrogen [TN]; however, Total Phosphorus [TP], Total Organic Nitrogen [TON], SiO_2, and NO_3^- all displayed a similar trend). For the simulated terrestrial boundary, TP was comprised of total inorganic phosphate and total organic phosphate. TN was determined by the summation of TON, NO3, NO2, and ammonia. In some instances, total carbon concentrations were not available; instead only total organic carbon concentrations were available. In order to use these data, the total organic carbon concentrations were assumed to be essentially the same as total carbon. Due to the lack of spatial and temporal coverage of water quality data for Charlotte Harbor in 1998 as well as to expand the available data set to create a more robust statistical relation-
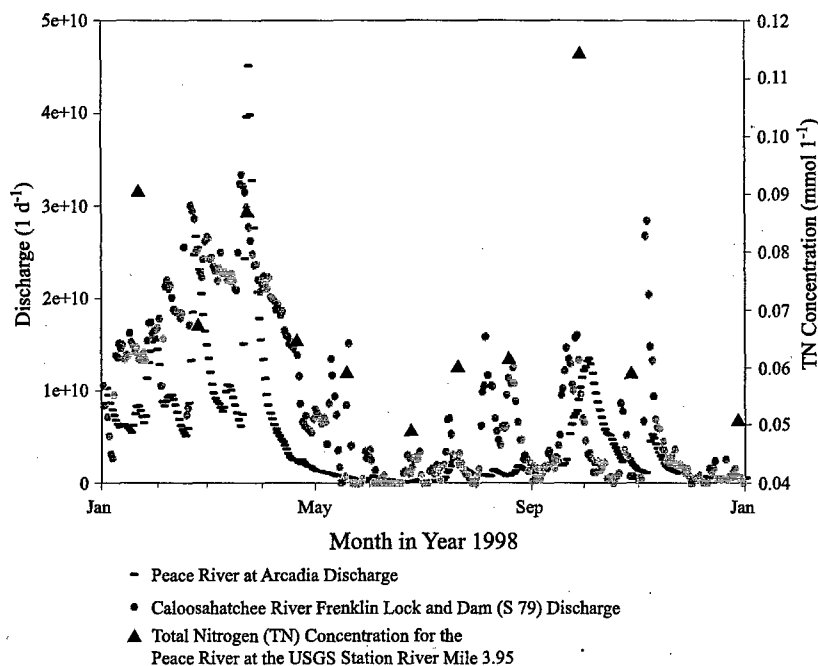
Fig. 2. Total daily discharge (1 d^{-1}) for 1998 from the Peace River measured at the USGS station "Peace River at Arcadia" and the Caloosahatchee River at the W.P. Franklin Lock and Dam (S79) and total nitrogen concentration [TN, (mmol l^{-1})] measured at the USGS station "Peace River at River Mile 3.95 near Punta Gorda, FL".

ship between nutrient and color concentrations as a function of salinity, data from the year 1999 were also included and evaluated in the creation of the shoreward boundary condition.

The shoreward boundary (approximately the 10-m isobath on the WFS) was assumed to have a salinity of 31.5; and therefore, regression analyses of nutrient data were interpolated at 31.5 (Table 1). Discharges originating from stations on the Peace or Caloosahatchee River with no given salinity values were assigned a salinity of 0.5. In order to utilize ECOHAB Process Cruise data not containing associated salinity values, station locations from the 40-m isobath and seaward were assigned a salinity value of 35. Data from ECOHAB stations shoreward of the 40-m isobath with no salinity data were omitted. Extreme outlying data points and negative values were excluded from evaluation.

The shoreward boundary conditions for the pulse case were simulated by an increase in nutrient and total color concentrations at the shoreward boundary model cell, from the surface to a depth of 10 m, reproducing a riverine flux. This location approx-

imates the EC-6 mooring as well as the minimum in bottom salinity of 31.5 during 1998. An accompanying freshwater flux and change in buoyancy is not simulated in the physical solution due to the 2D nature of this model. The physical constraints made it impractical to hydrologically model the freshwater

Table 1
The organic and inorganic nutrients present in the Charlotte Harbor region and on the WFS during 1998 and 1999

	Data interpolated at a salinity of 31.5 (μmol l^{-1})
Si	9.46
o-PO$_4$	0.512
NH$_4$	1.309
NO$_3$	0.947
TN	22.31
TC	406.285
organic P	1.3
TP	1.812
TON	17.364
chl (μgl^{-1})	2.512

Shoreward boundary conditions are determined by regression analysis to a salinity of 31.5.

mass. It is clear that the baroclinic flows would be altered by these events; however, it is beyond the scope of this effort to predict those impacts. The shoreward boundary conditions, for the pulse case, were simulated by the addition of the mass constituents and concomitant optical signal, estimated from Table 1 on DOY 267 and 309 (the actual values and state variable into which these mass constituents were added are given in Table A.5). This is possibly a conservative estimate of the ecologically significant mass additions to the shelf during these periods, as the outflow events driving the decreases in salinity would have occurred over the course of several days (or possibly weeks) as revealed by the bottom mounted mooring (10-m depth) located adjacent to Charlotte Harbor (Ocean Circulation Group, 2004).

3.4. SeaWiFS processing

All SeaWiFS imagery processing from High Resolution Picture Transmission (HRPT) data to total chlorophyll, detrital and gelbstoff absorption [a_{dg}(412 nm)], and backscattering [b_b(555 nm)] was performed at NRL-Stennis by the Ocean Sciences Branch, Code 7330. Standard SeaWiFS protocols were applied for calibration and navigation. Atmospheric correction used a modified (Gordon and Wang, 1994) procedure designed for coastal waters with nonzero water leaving radiance in channels 7 (765 nm) and 8 (865 nm; Arnone et al., 1998). This procedure iteratively solves for the correct water-leaving radiance values in channels 7 and 8 in coastal waters where particulate scattering may yield significant upwelling light from the sea surface. The data were then processed using the biooptical algorithms for a_{dg}(412) (Carder et al., 1999), total chlorophyll (OC4, O'Reilly et al., 1998), and b_b(555) (Gould and Arnone, 1998).

Data, stored as one byte per pixel, were then gridded, averaged, and binned by day. This image is a byte-valued, 2D array of a Mercator projection of South Florida. Each product contains one image of a geophysical parameter and is stored in one physical hierarchical data format file. The region of interest on the WFS originated at the 10-m isobath and extended approximately 60 km offshore. The boundary of the region was designated by the coordinates

[(27.2957N, 83.3415W), (27.5396N, 82.7993W), (26.2062N, 82.7200W), (26.4502N, 82.1830W)] (Fig. 1). Lines of data were sampled at 30 equally spaced intervals between these points using the SeaWiFS Data Analysis System (SeaDAS). The mean of these 30 lines (numbered from Tampa Bay south to Charlotte Harbor) and the mean plus and minus one standard deviation were then plotted. The mean of lines 22–30 (near Charlotte Harbor) were also plotted since this location is the focus of the study.

4. Results

Fig. 3 illustrates the results from the physical circulation model for the months of June and November. For 10 months of the year, the simulated water flow was predominately down the coast, and onshore at the bottom, offshore at the surface. This would approximate upwelling conditions with a Loop Current intrusion at the 40-m isobath. The exceptions to this type of simulated flow were during the months of April and September where up coast, onshore at the surface, offshore at depth conditions prevailed, approximating downwelling conditions at the coast. These conditions for the fall of 1998 mirror a more robust 3D study of the WFS (He and Weisberg, 2002a) and suggest that the 2D solution may provide a reasonable estimate of the cross-shelf flows during the summer and fall events of this simulation.

The comparison between simulated and satellite-derived optical properties focuses on the days where there were good quality SeaWiFS images for the West Florida Shelf. The days chosen here were June 8th and November 8th. While there were other days during the end of 1998 that provide clear satellite imagery, the chosen days provided data of significant ecological events that were evident in the available in situ data (not all collected in situ data from the region were processed and available to this research group at the time of this publication). The June 8th image was collected during the simulated and measured increase in biomass resulting from the Loop Current intrusion. The November 8th image marked a period just after a significant pulse of freshwater from the Peace and Caloosahatchee

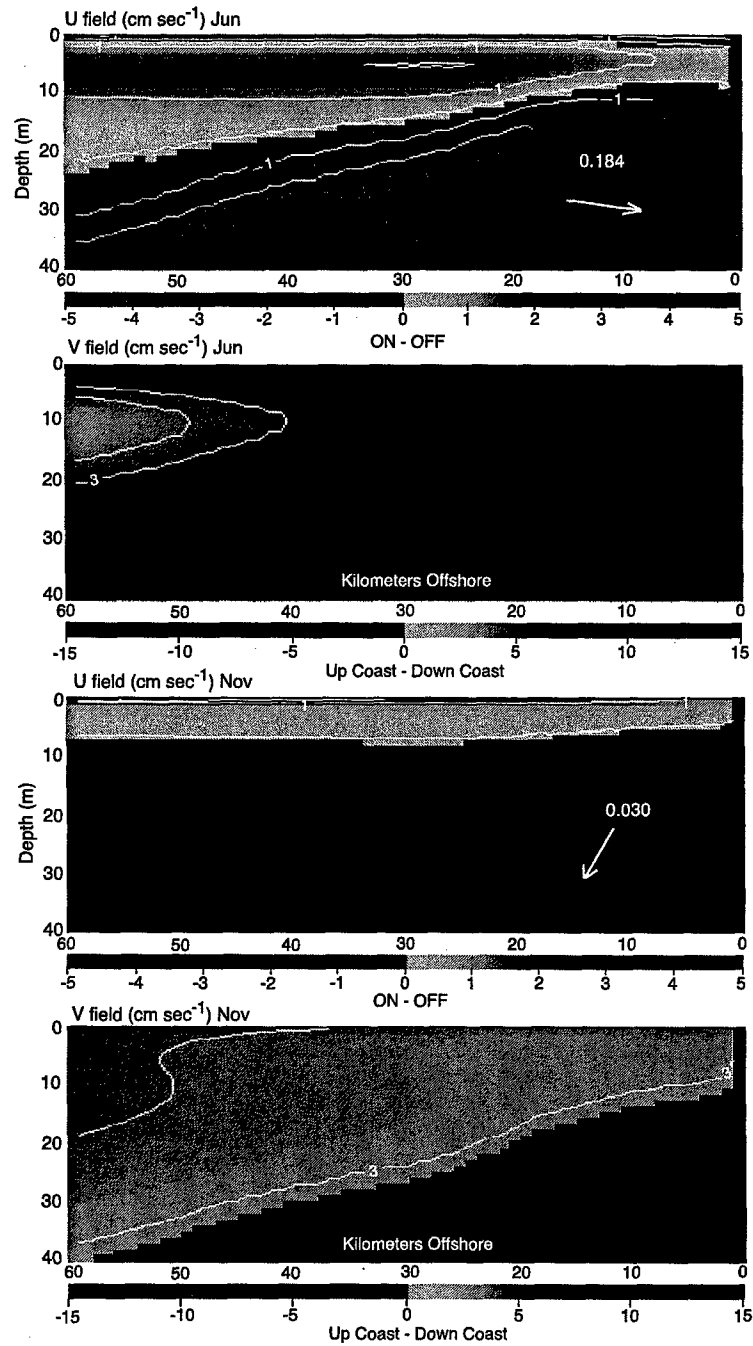Fig. 3. The 2D physical circulation model displaying the directional velocity fields of U field (cm s^{-1}) and V field (cm s^{-1}) for June and November 1998. Directionality is as follows, up coast is north (into the page) whereas down coast is south (out of the page).

Rivers. During periods of significant discharge (in particular, November and December), releases from the rivers lasted several days to several weeks. The simulation results discussed herein consist of two separate simulation cases (from over 80), where the only differences between Case 1 and Case 2 were the addition of the pulse conditions on DOY 267 and 309 (Case 2), coinciding with Hurricanes Georges and Mitch. Table 2 gives an overview of the simulated and satellite-derived means and variances of the IOPs across the shelf on June 8 and November 8 for the average of the SeaWiFS entire domain at the surface, the average of the SeaWiFS Charlotte Harbor lines at the surface, and the EcoSim Case 1 (no-pulse) and Case 2 (pulse) averaged for the top 5 m of the water column over the entire domain.

4.1. June 8—DOY 159

An upwelling event due to an intrusion by the Loop Current prevailed over the WFS and was detected by satellite imagery exemplified by slightly elevated offshore detritus and CDOM absorption [a_{dg}(412 nm) Carder algorithm; Fig. 4a] and chlorophyll a (OC4 algorithm; Fig. 4b) in June 1998. This upwelling event was not apparent in the backscatter imagery derived from SeaWiFS [b_b(555 nm) Arnone algorithm; Fig. 4c]. The satellite-derived detritus and CDOM absorption, total chlorophyll, and backscatter

(Fig. 5a–c, respectively) averaged over the entire domain and Charlotte Harbor lines show slightly elevated nearshore values with a declining gradient offshore. Slightly elevated values are noted in the surface waters of all the simulated IOPs approximately 20 to 45 km from the shoreward boundary. The slight elevation in the nearshore satellite-derived CDOM signal, chlorophyll a, and backscatter are indicative of a riverine source and are not present in the simulated cases due to a lack of a pulse event. The generation of slightly elevated simulated offshore values correlates with a sampled and recorded chlorophyll event by the ECOHAB Process Cruise with a maximal measured chlorophyll concentration, 6.58 mg chl m^{-3}, recorded at ECOHAB Station 34 (26.99N, 82.7467W) at a depth of 20 m approximately 12 km from the shoreward boundary on June 11, 1998. Although the transport of this upwelled event occurred at depth, it may have been visible in surface satellite images; however, it was difficult to pin point it in the satellite imagery.

No strong differences were observed between Case 1 and 2 on June 8 because this date was prior to the simulated pulse releases (Table 2; Figs. 5 and 6). The simulated surface and 5 m average values for Case 1 and 2 displayed fairly steady trends from nearshore to offshore, with the magnitude of the results for the average of the top 5 m of the water column exhibiting greater values than at the surface (Fig. 5a–c). The

Table 2

The mean and variance of simulated and satellite-derived detritus and CDOM absorption [a_{dg} 412 nm (m^{-1}), Carder algorithm], Total Chlorophyll [chl–OC4 algorithm (mg chl a m^{-3}), and backscatter (b_b 555 nm (m^{-1}), Arnone algorithm] on June 8, 1998 (DOY 159) and November 8, 1998 (DOY 312)

		June 8 (DOY 159)				November 8 (DOY 312)			
		Entire domain	Charlotte Harbor lines	EcoSim Case 1	EcoSim Case 2	Entire domain	Charlotte Harbor lines	EcoSim Case 1	EcoSim Case 2
a_{dg}	Mean	0.067	0.069	0.056	0.056	0.089	0.098	0.059	0.093
	Variance	6.58E-05	4.70E-05	4.69E-06	4.67E-06	2.05E-03	2.58E-03	1.31E-04	6.87E-03
chl	Mean	0.954	0.906	0.497	0.503	1.104	1.426	0.628	1.008
	Variance	6.92E-02	3.62E-02	1.56E-03	1.62E-03	6.54E-01	9.26E-01	6.63E-02	9.82E-01
b_b	Mean	0.0044	0.0040	0.0023	0.0023	0.0061	0.0104	0.0026	0.0030
	Variance	6.55E-07	1.04E-06	1.38E-08	1.41E-08	2.32E-05	8.51E-05	2.63E-07	1.37E-06

Satellite-derived values for the SeaWiFS entire domain at the surface were determined by the following coordinates: (27.2957N, 83.3415W), (27.5396N, 82.7993W), (26.2062N, 82.7200W), (26.4502N, 82.1830W). Data were sampled at equal intervals across this domain, resulting in a total of 30 parallel lines. The Charlotte Harbor lines were designated as lines 22 through 30, numbered from north to south. The simulated results are for the EcoSim Case 1 (no pulse) and EcoSim Case 2 (pulse) averaged for the top 5 m of the water column over the entire domain (region mentioned above).
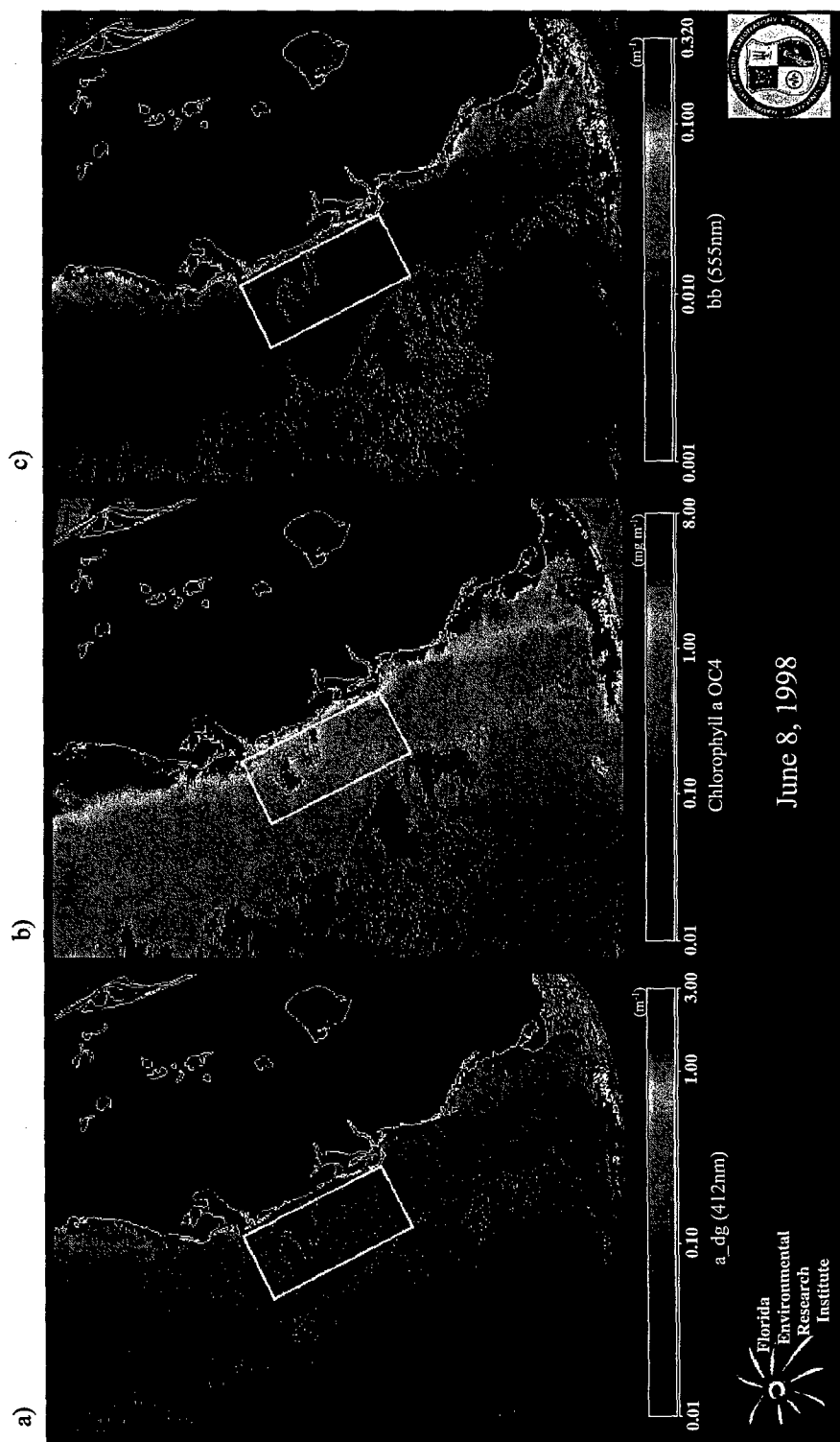
Fig. 4. SeaWiFS imagery of the WFS on June 8, 1998. The white box denotes the boundaries of the EcoSim 30 parallel lines [(27.2957N, 83.3415W), (27.5396N, 82.7993W), (26.2062N, 82.7200W), (26.4502N, 82.1830W)]. (a) Detritus and CDM absorption (a_{d_g} 412 nm) Carder algorithm; (b) total chlorophyll a (OC4 algorithm); (c) backscatter (b_b 555 nm) Arnone algorithm.
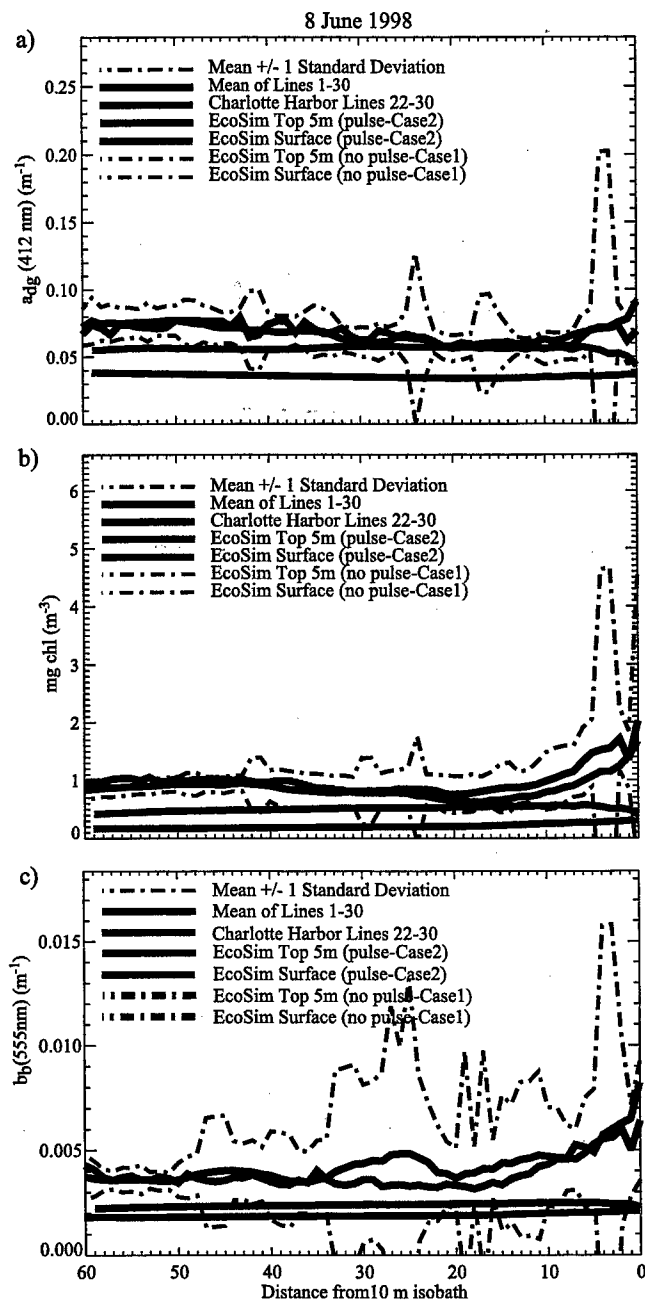
Fig. 5. Simulated and satellite-derived IOPs on the WFS on June 8, 1998. (a) detritus and CDM absorption [a_{dg} 412 nm (m^{-1})]; (b) total chlorophyll concentration (mg chl m^{-3}); and (c) backscatter [b_b 555 nm (m^{-1})] on the WFS displaying the mean of the 30 lines transect, +/−one standard deviation of the mean of 30 lines, the mean of lines 22–30 (Charlotte Harbor), and Case 1 and 2 simulated absorption (5 m average and at the surface). The nearshore boundary is approximately the 10-m isobath on the WFS, and the boundary conditions were derived from nutrient data collected during 1998 and 1999.

Case 1 - No Pulse

Case 2 - Pulse
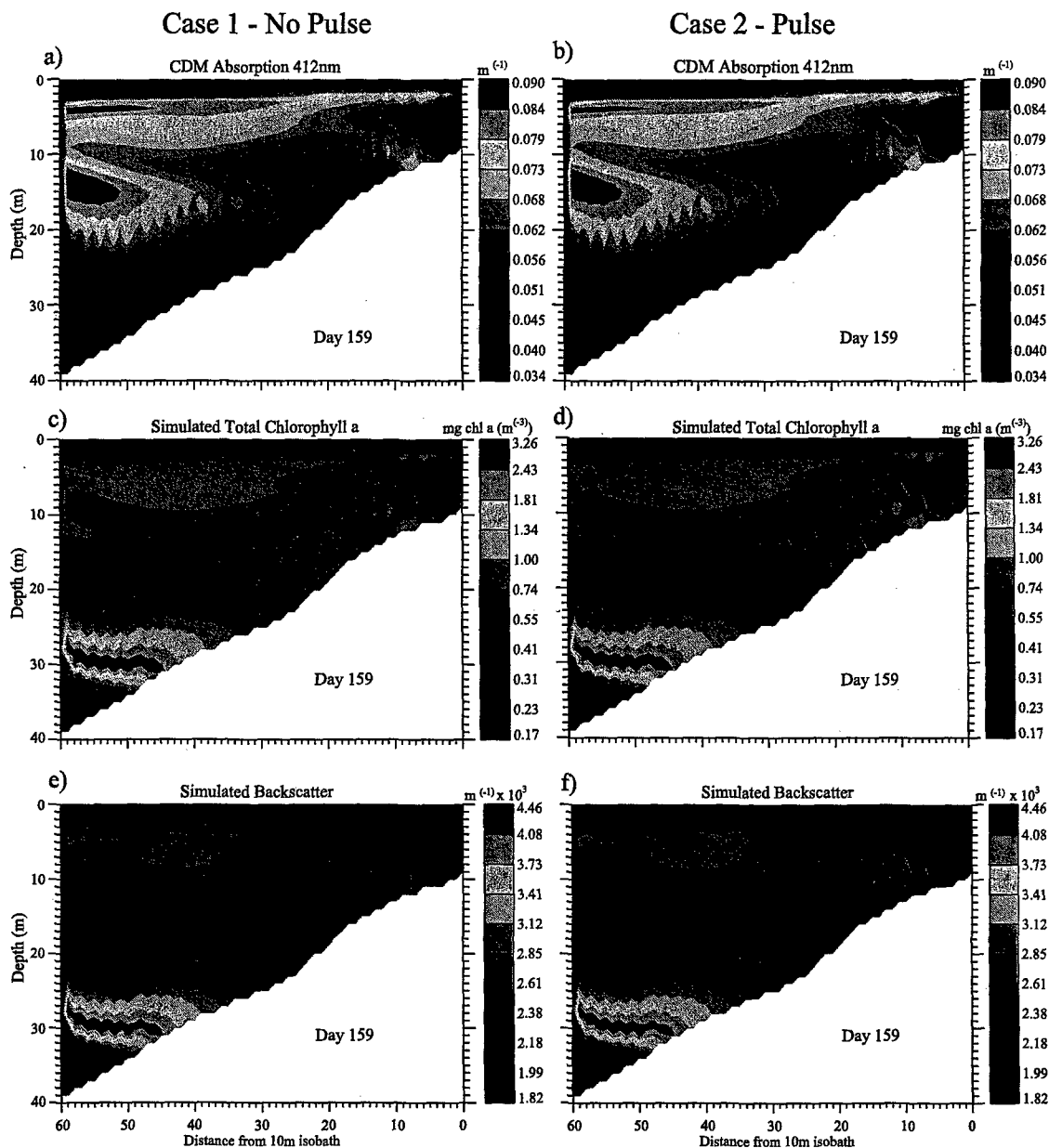
Fig. 6. Simulated vertical structure of the IOPs from EcoSim for the entire domain (a) CDM absorption (m^{-1}) for Case 1; (b) CDM absorption for Case 2; (c) total chlorophyll a concentration (mg chl m^{-3}) for Case 1; (d) total chlorophyll a concentration for Case 2; (e) backscatter (m^{-1}) for Case 1; and (f) backscatter for Case 2 on the WFS on June 8, 1998 (calendar day 159).

slight cross-shelf gradient present in the satellite-derived data, likely due to a spring freshwater pulse (Fig. 2), was not simulated and hence not observed in the modeled data. Beneath the surface layers, the

simulated absorption increased significantly, showing peaks at both 5- and 15-m depths 30 to 60 km from the shoreward boundary (Fig. 6a,b) corresponding to the upwelling event. The simulated vertical structure

of both the total chlorophyll concentration (Fig. 6c,d) and backscatter (Fig. 6e,f) display similar trends with regions of elevated values offshore at depth corresponding to the upwelling event (maximal simulated chlorophyll concentration was 3.26 mg chl a m^{-3} and maximal simulated backscatter value of 0.00446 m^{-1}). There were also simulated regions of slightly elevated chlorophyll concentration (0.74–1.00 mg chl a m^{-3}) and backscatter (0.00285–0.00312 m^{-1}) offshore less than 10 m deep.

Despite a lack of a slight cross-shelf gradient in the modeled results, the simulated IOPs were generally within one standard deviation of the mean of the entire domain with the exception offshore where the simulated surface values were generally below this constraint. As mentioned above, there was no flux of nutrients and color from the shoreward boundary condition during this time of the year. While the actual flows were low out of Charlotte Harbor region compared to the high flux events during the fall, they were not zero (Fig. 2), possibly suggesting the relative importance of fresh water fluxes to the surface IOPs throughout the year. The subsurface results revealed the generation of an offshore upwelling event similar to that sampled by the ECOHAB Process Cruise on the WFS in June 1998. The spatial profile of this modeled event appeared to be deeper and further offshore than the recorded event, likely a constraint of the physical forcing of the model.

4.2. November 8—DOY 312

Tropical Storm Mitch (downgraded to a Tropical Storm from a Hurricane just before moving onshore) made landfall on the west coast of Florida near Naples on November 5, 1998. The Page Field Airport in Fort Myers, Florida reported 6.05 in. of rainfall on November 5 (http://www.nhc.noaa.gov/). This enormous amount of rainfall led to massive releases from the Peace and Caloosahatchee Rivers (Fig. 2; W.P. Franklin Lock and Dam (S79)) over the course of several days. Our simulated pulse was strictly limited to a release on November 5, possibly underestimating the total flux of freshwater and nutrients.

With only the June Loop Current intrusion on the WFS to force nutrient and color fluxes, the Case-1-simulated results fail to replicate the cross-shelf

gradient observed by satellite imagery (Fig. 7a–c) and ECOHAB sampling in November of 1998. Simulated Case 1 surface and nearsurface CDOM absorption, total chlorophyll concentration, and backscatter (Fig. 8a–c, respectively) remained virtually constant across the shelf. Since no terrestrial inputs were simulated in Case 1, simulated backscatter remained almost static across the shelf. Simulated subsurface results displayed negligible CDM absorption (Fig. 9a) throughout the water column. Regions of moderately elevated chlorophyll concentrations, 2.78 to 3.94 mg chl a m^{-3} (Fig. 9c), and backscatter, 0.0043 to 0.0048 m^{-1} (Fig. 9e), were present offshore at depth with slightly less elevated values of 5–20 km from the shoreward boundary. The cross-shelf gradient for the simulated no-pulse case was minimal compared to the pulse case, reinforcing the fact that the ecological events present during the fall of 1998 near the shoreward boundary were likely due to the input of terrestrial nutrients.

When terrestrial inputs were introduced at the shoreward boundary, the simulated IOPs corresponded well with observed results. The average detritus and CDOM absorption estimated by Sea-WiFS imagery showed a declining trend from onshore to offshore (Fig. 7a). The simulated pulse event was exemplified by a strong cross-shelf gradient in CDOM absorption (Fig. 8a). Nearshore at the surface, absorption (0.615 m^{-1}) exceeded the 5 m average absorption for Case 2 (0.400m^{-1}); however, offshore, the surface absorption estimates were slightly below the simulated 5 m average. The simulated pulse case nearshore values were of a greater magnitude than the average for the entire domain and for the Charlotte Harbor lines (Table 2 and Fig. 8a–c). Yet, offshore-simulated absorption values were more in line with the satellite-derived absorption values over the entire domain. The vertical structure of Case-2-simulated absorption displayed a nearshore maximum at the surface of 0.615 m^{-1}, rapidly declining offshore with depth (Fig. 9b, note that the scales of Fig. 9a and b are different).

The cross-shelf trend was also observed for chlorophyll concentration on the WFS (Fig. 8b). The Case-2-simulated chlorophyll concentration for the upper 5 m of the water column mimics the satellite estimates; although the simulated nearshore surface results
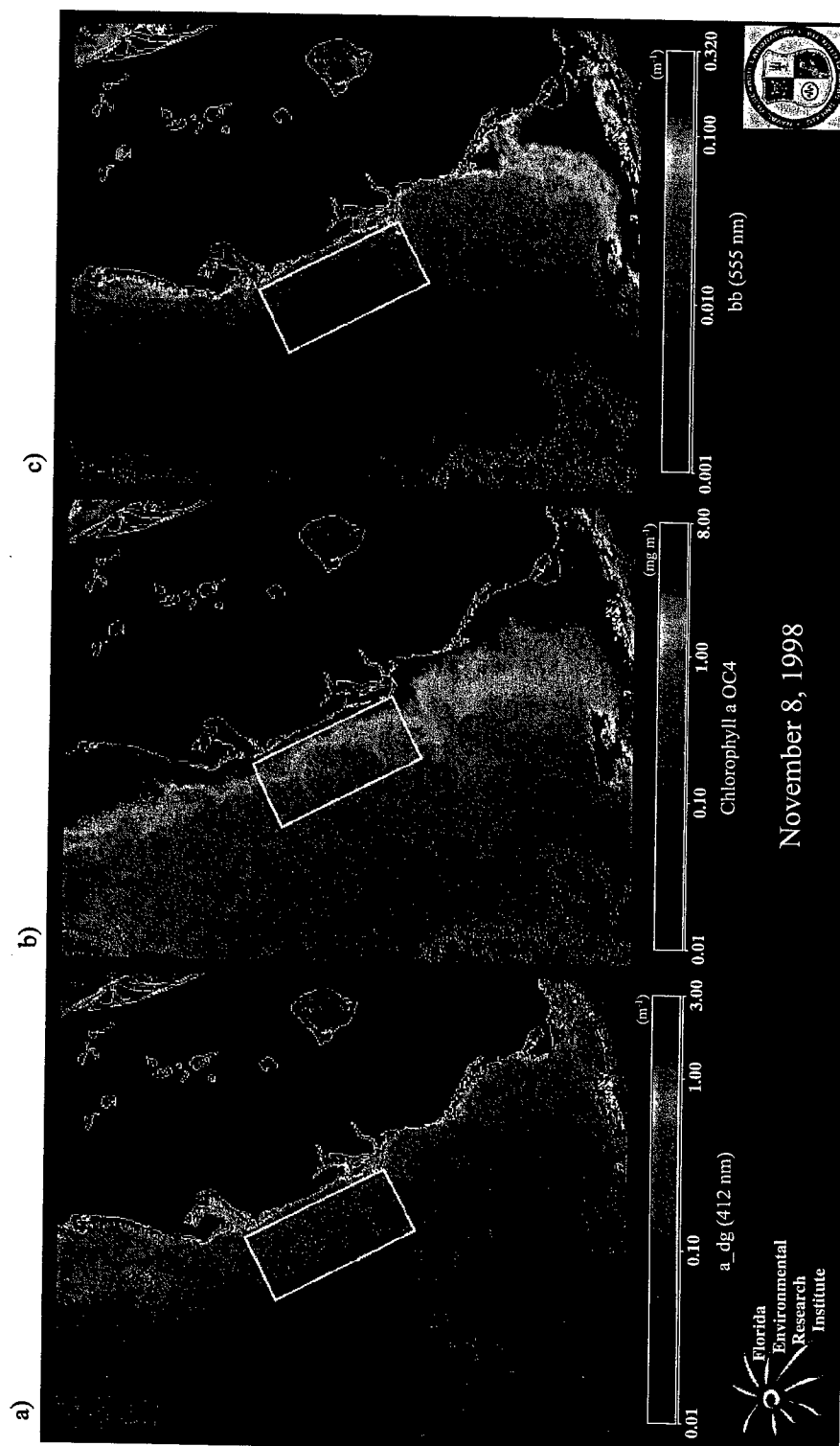
Fig. 7. SeaWiFS imagery of the WFS on November 8, 1998. White box denotes the boundaries of the EcoSim 30 parallel lines [(27.2957N, 83.3415W), (27.5396N, 82.7993W), (26.2062N, 82.7200W), (26.4502N, 82.1830W)]. (a) Detritus and CDM absorption (a_{d_g} 412 nm) Carder algorithm; (b) total chlorophyll a OC4 algorithm; (c) backscatter (b_b 555 nm) Arnone algorithm.
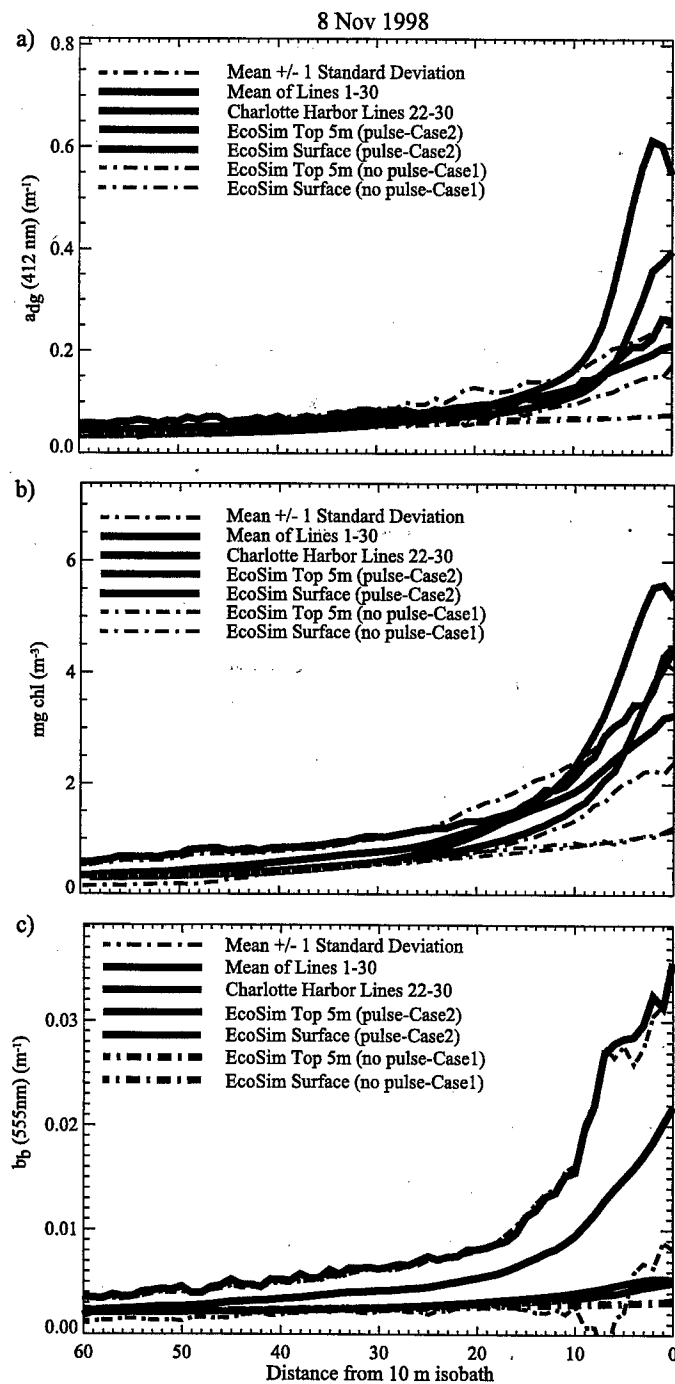
Fig. 8. Simulated and satellite-derived IOPs on the WFS on November 8, 1998. (a) Detritus and CDM absorption [a_{dg} 412 nm (m^{-1})]; (b) total chlorophyll concentration (mg chl m^{-3}); and (c) backscatter [b_b 555 nm (m^{-1})] on the WFS displaying the mean of the 30 lines transect, +/– one standard deviation of the mean of 30 lines, the mean of lines 22–30 (Charlotte Harbor), and Case 1 and 2 simulated absorption (5 m average and at the surface). The nearshore boundary is approximately the 10-m isobath on the WFS, and the boundary conditions were derived from nutrient data collected during 1998 and 1999.

slightly exceed the satellite-derived estimates. The vertical structure for Case 2 chlorophyll displayed a maximal nearshore concentration of 5.59 mg chl a m^{-3}, approximately 0 to 3 m deep gradually declining offshore (Fig. 9d). The region of slightly elevated

chlorophyll concentration observed offshore at depth, noted in Case 1, was also present in Case 2 results.

The cross-shelf gradient in SeaWiFS satellite-derived backscatter was observed for both the entire region and the Charlotte Harbor lines (Fig. 8c). With
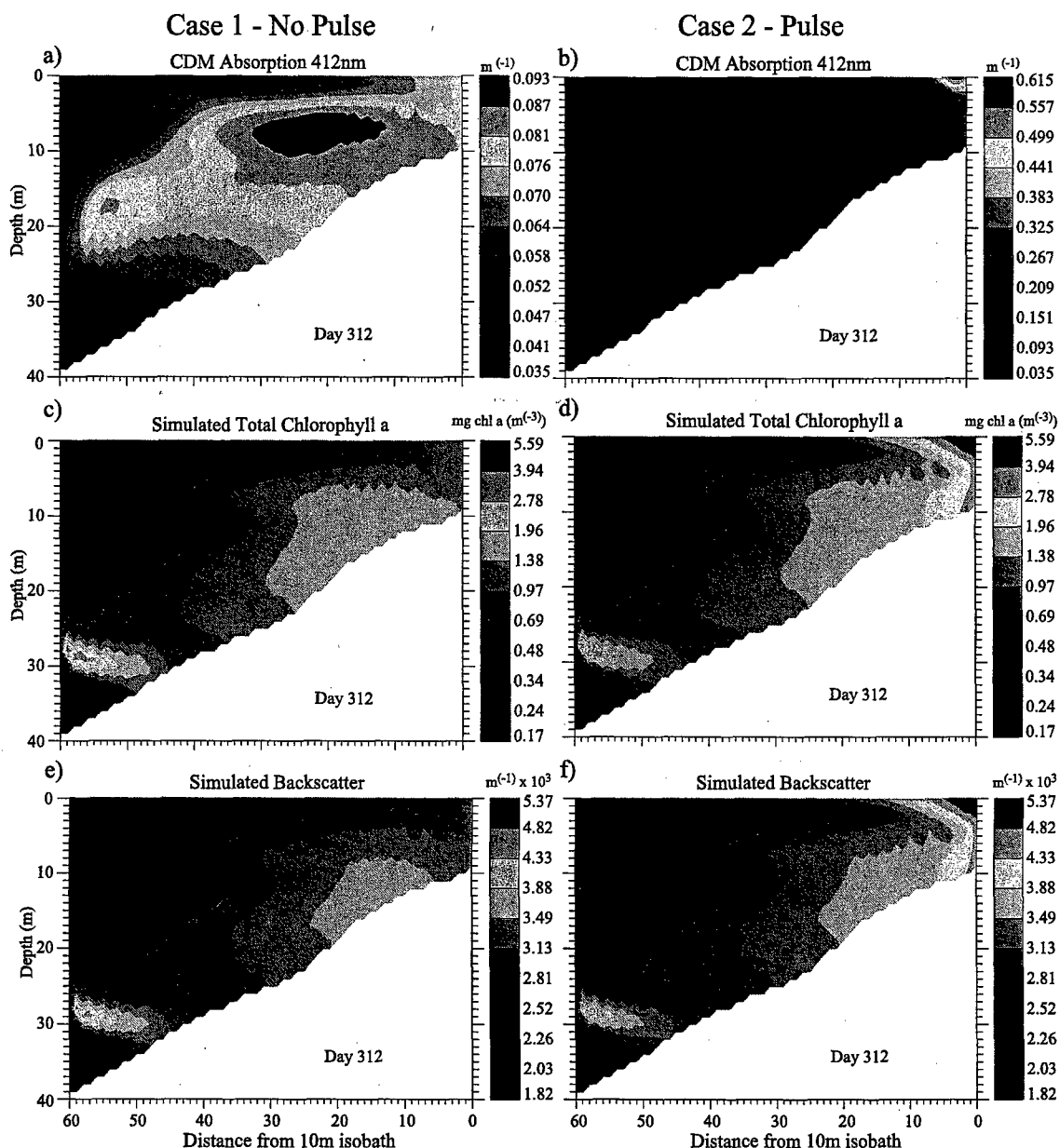
Fig. 9. Simulated vertical structure of the IOPs from EcoSim for the entire domain (a) CDM absorption (m^{-1}) for Case 1 (note: Case 1 and 2 use different scales); (b) CDM absorption for Case 2; (c) total chlorophyll a concentration (mg chl m^{-3}) for Case 1; (d) total chlorophyll a concentration for Case 2; (e) backscatter for Case 1 (m^{-1}); and (f) backscatter for Case 2 on the WFS on November 8, 1998 (calendar day 312).

the addition of terrestrial inputs, Case-2-simulated backscatter paralleled the onshore to offshore gradient of the satellite estimates, however, to a lesser extent. Case-2-simulated backscatter exhibited a maximal value of 0.0054 m^{-1} nearshore, approximately 0 to 3 m deep gradually waning offshore (Fig. 9f). The noted offshore peak in backscatter at depth in Case 1 was also present in Case 2 results.

The simulated nearshore increases in absorption, chlorophyll, and backscatter were confirmed not only by satellite imagery but also by ECOHAB Process Cruise D data from November 16–19, 1998. The freshwater pulses released into Charlotte Harbor (November 4–22) were also visualized by ECOHAB Process Cruise sampling of the region. Regions of lower salinity water (30–33, compared to the surrounding waters) were sampled by the ECOHAB Process Cruise as they emerged from the barrier islands of Charlotte Harbor (Fig. 10). Regions of high chlorophyll fluorescence (as high as 10 μg chl
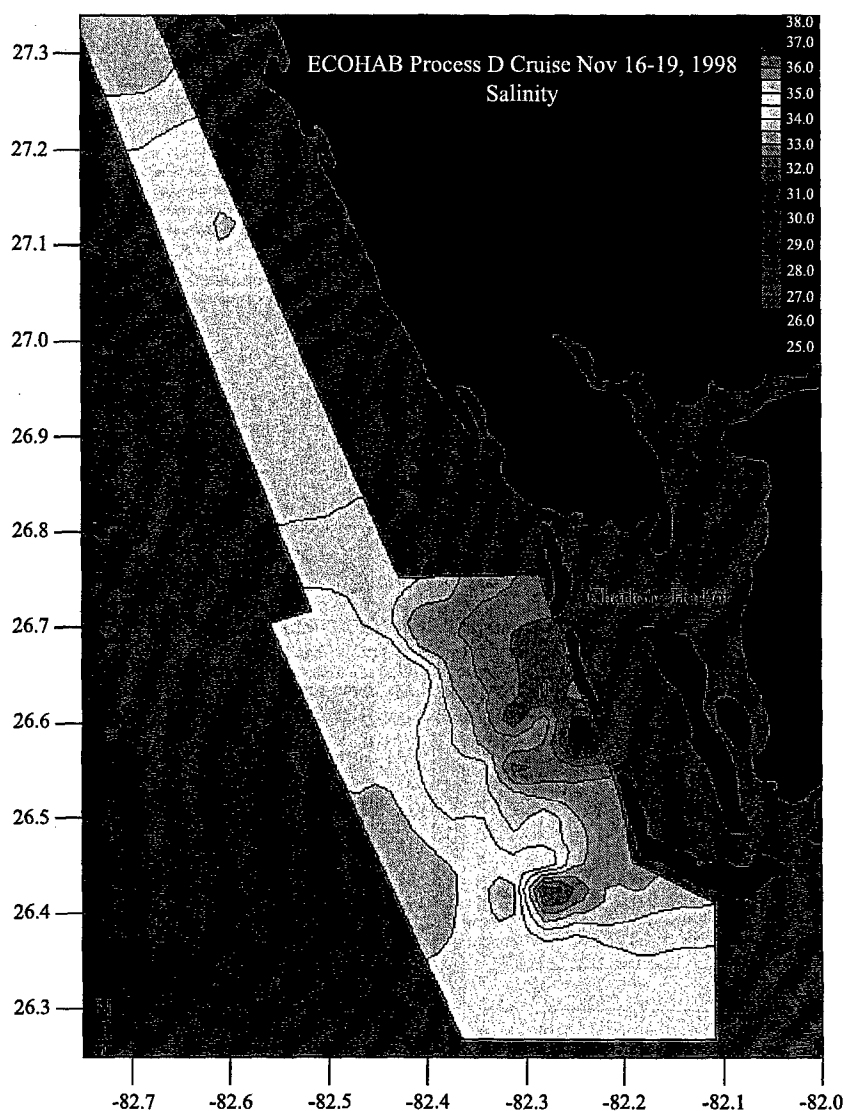
Fig. 10. Salinity measured near Charlotte Harbor during the ECOHAB Process D Cruise on November 16–19, 1998.

1^{-1}; Fig. 11) were colocalized with regions of lower salinity. SeaWiFS imagery on November 8th also displayed a region of elevated chlorophyll near Charlotte Harbor (Fig. 7b) that correlates to a maximal surface chlorophyll concentration of 1.14 mg chl m^{-3} (data not shown) observed during the ECOHAB Cruise. These in situ samples provide further evidence that (1) nearshore salinity fronts, likely due to enhanced runoff and riverine discharges, were present in the region and (2) regions of elevated chlorophyll were colocalized with areas of lower salinity water. These elevated chlorophyll concentrations may be driven by in situ production derived from elevated nutrient concentrations or
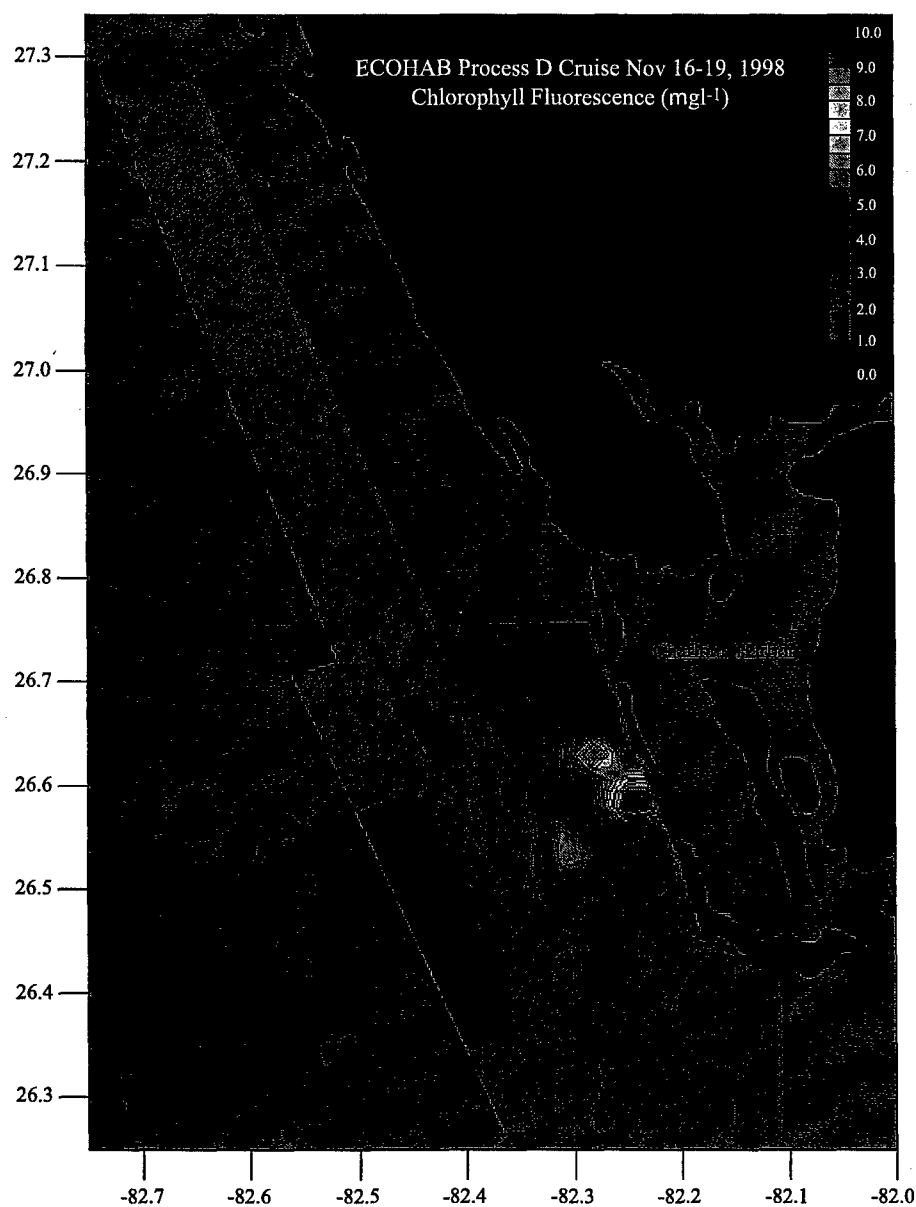

Fig. 11. Chlorophyll fluorescence ($\mu g l^{-1}$) sampled near Charlotte Harbor during the ECOHAB Process D Cruise on November 16–19, 1998.

may simply be washed out chlorophyll from the estuary. In either case, the organic supply of total nutrients in DOM or POM form would drive increased production after regeneration of the DOM/POM pools, with a concomitant increase in biomass accumulation.

It should be noted that, on an annual basis most of the CDM (sum of $CDOC_1$ and $CDOC_2$), color was produced via in situ ecological processes with an increase in total annual integrated CDM between Case 1 and Case 2 of 22.4%; however, only 53.4% of this increase (12.0% of the total annual integrated CDM) in CDM concentration was the result of direct CDM additions at the boundary. The remaining increase in CDM was driven by additional ecological interactions that resulted from increases in DOM and nutrients at the terrestrial boundary. These color addition estimates may be on the low side, as the terrestrial boundary conditions were simulated with just two pulses of nutrients and color on DOY 267 and 309. There may have been a more continuous supply of terrestrial nutrients and organic color. In both cases, >80% (83% and 87% Case 1 and Case 2, respectively) of the total CDM was removed via advection out of the model domain.

As previously mentioned, over 80 simulations were completed. While details of all of these simulations are beyond the scope of this paper, the results from one simulation were particularly relevant to this study. In this additional simulation study, photolysis and photochemical reductions were set to zero (Case 0-Photo), and all other parameters and forcing were held as in the pulse case, Case 2 (as previously described). The average annual percent reduction in total CDM concentration between the Case 2 and 0-Photo simulations was 3.05%, reflecting the photochemical removal of CDM in the Case 2 simulation. On DOY 159 and 312, these percent differences were −5.15% and −3.90%, respectively.

These increases in CDM concentrations in the 0-Photo simulation yielded small increases in spectral absorption and small decreases in downwelling irradiance. The average percentage decrease in integrated E_d between the Case 2 and 0-Photo simulations was 1.49%. On DOY 159 and 312, these percent differences were −1.37% and −2.57%, respectively. This reduction in Case 0-Photo E_d was matched by a

decrease in total primary production. Integrated primary production for the Case 0-Photo year decreased by 0.21%; and on DOY 159 and 312, integrated primary production dropped 0.10% and 0.91%, respectively.

5. Discussion

The ability to predict the IOPs of the water column is crucial in the effort to forecast or hindcast model the ecological state of the water column. IOPs are properties of the water column (absorption, beam attenuation, and scatter) that are independent of the geometry of the ambient light field. The IOPs of the water column may be directly related to the concentration and composition of dissolved and particulate materials of the oceans and may provide the means to tie numerical state variables to measurable quantities of water clarity and quality, underwater visibility, particle composition, and primary production by phytoplankton. The interrelationship between AOPs and IOPs is of critical importance. If one can predict the IOPs of the water column and couple these predictions with robust radiative transfer models, then one can predict AOPs such as attenuation and scalar irradiance. The interactions between IOPs and AOPs provide the means to approximate water column visibility and primary productivity when directly coupled with an ecological model that simulates spectral absorption and quantum yield as a function of light and nutrients (Bissett et al., 2001). This paper lays the groundwork for hindcast modeling based on a series of experiments conducted on the West Florida Shelf in 1998. Two companion papers will follow, one focusing on the phytoplankton composition (Bissett et al., 2003) and another exploring the fitness of the IOP model when combined with a more robust radiative transfer model (Mobley, 1994) for predicting the AOPs (Bissett et al., 2004a) on the WFS during 1998. A key point to this current work is that it does not focus on a reductionistic viewpoint of modeling, choosing only a minimal set of parameters and interaction equations to match a specific validation data set. Instead, the focus was to try to build a framework that would address both ocean color and ecology across transition zones (ecotones)

and will therefore be more applicable to both coastal and open ocean solutions. The goal was to develop an ecological framework that may be nested into larger physical models, which may then span from basin to estuary solutions.

The typically oligotrophic WFS is a complex 4D biogeochemical system that is affected by episodic intrusions of the Loop Current, periodic terrestrial inputs from freshwater sources, and possible organic nitrogen supplied by nitrogen fixing cyanobacteria. The faithfulness of a model simulation to replicate the intricate balance of physical, biological, chemical, and optical constituents of the coastal ocean is dependent on accurately predicting each of these components. An open ecological ocean model developed by Bissett et al. (1997) was modified for this nearshore environment. The complexity of this enhanced ecological model may not fully be displayed in the context of the modeled results presented herein. The purpose for such a model is to implement a realistic simulation of the IOPs, phytoplankton species, and the remote sensing reflectance present on the WFS, so as to assist in the prediction of the biogeochemical processes present during extreme ecological events, i.e., black water or harmful algal blooms. All of the mathematical variables and functions presented herein may seem superfluous when narrowly focused on the effects of CDOM on the WFS; however, the generation of this robust model conserves time and resources by permitting the concurrent modeling of the IOPs, AOPs, biological, and ecological state of the water column. This multivariate model can be used by a broad range of disciplines from ecological modeling to biogeochemistry to the study of remote sensing.

The ecological and optical results from this simulation are directly dependent upon the physical circulation model. It is clear that the WFS is a 4D system (x, y, z, t; He and Weisberg, 2002a; He and Weisberg, 2002b; Walsh et al., 2002; Walsh et al., 2001), and its representation by a reduced dimension system (x, z, t) will introduce uncertainties that make exact comparisons to in situ data difficult. A direct correlation study is thus difficult because the physics and boundary conditions drive the 0- and 1st-order solutions. Significant errors in the physics and boundary conditions will drive errors outside of the

ecological coding. We seek to focus on two events that will help focus on the "reasonableness" of the ecological and optical results in light of the simulated physical forcing and hopefully provide information on the applicability that this ecological and optical solution may have to the fully 4D WFS system. The tests used here focus on the magnitude, time-lag biomass, and optical property responses to physical events compared to measured data with similar hydrographic profiles as well as statistical comparisons between SeaWiFS-derived and simulated surface pigments and optical properties.

The simulated biomass distribution and optical constituents on the shelf are in good agreement with observations in June. A simulated Loop Current intrusion, represented by higher nutrient boundary conditions coupled with along- and cross-shore transport, led to an accumulation of biomass, which appeared to be similar to an ECOHAB-sampled biomass peak. Nutrients from this modeled event entered the model domain below 25 m (Fig. 3) at a stoichiometric ratio of Si/N/P of ~14:14:1. The sampled ECOHAB event showed chlorophyll stocks reaching 6.58 mg chl m^{-3} on June 12, 1998 (26.99 N, 82.75 W, ECOHAB station 34) at a depth of 20 m–27 km from the 10-m isobath. The maximum simulated chlorophyll at depth on this day was ~3.3 mg chl m^{-3}, found further offshore (Fig. 6c,d). However, by mid-July, the maximum simulated chlorophyll from the intrusion reached ~7.6 mg chl m^{-3} at a depth of 22 m, 30 km from the 10-m isobath (data not shown), suggesting a temporal difference in the simulated supply of nutrients and the increase in chlorophyll biomass associated with the measured Loop Current intrusion.

The Loop Current intrusion was simulated here as strictly an offshore–onshore phenomenon; however, the exact location of this intrusion may have been farther to the north, with a subsequent transport down the coast (Walsh et al., 2003). This, coupled with the possible surface water flux from the north, suggested that the history of the 3D measured water mass may have been different than that of the simulated 2D mass, with possible differences in phytoplankton composition and biomass. These effects would cause discrepancies between the simulated solutions and the satellite estimates. Unfortunately, the entire ECOHAB data set was not available for evaluation; the data set

available to us for depth profile comparisons was very sparse, and we did not have the means to compute advanced statistical analyses over spatial or temporal scales. However, we look forward to performing a complete statistical analysis of our simulated results with this data set when it becomes available.

A slight cross-shelf gradient observed in the satellite imagery during June was indicative of a nearshore input of color particulate and dissolved organic matter as well as sediments (elevated b_b 555). This may have been in response to a large spring discharge event (Fig. 2) associated with elevated total nitrogen in the Peace River. Since this event was not simulated (nor any other spring and summer terrestrial events), the simulated results show no near surface cross-shelf gradient in IOPs. It would appear that a 4D solution to color dynamics on the WFS would need to include a more robust temporal solution for the shoreward boundary condition than was included in this simulation experiment.

Other differences between simulated surface and derived satellite IOPs could have been the product of subsurface features that may have impacted the remote sensing data (a follow-up manuscript will describe the impacts of the vertical structure of the simulated IOPs on the remote sensing reflectance signal; Bissett et al., 2004a). The discrepancies may also be more of a function of the overall physical solution of the model. In addition, there appeared to be a continuous mass of surface water from the north with increased colored absorption and chlorophyll about 50 km from the shoreward boundary (Figs. 4a,b and 5a). It is interesting to note that there was a SeaWiFS backscattering peak that corresponded to the peak in measured chlorophyll approximately 27 km from the shoreward boundary, yet this was not noted in the SeaWiFS estimates of chlorophyll a. This may suggest a difference in optical depth sensitivity between the SeaWiFS backscatter and chlorophyll algorithms.

Elevated nearshore CDOM measured by AC-9 data from the October ECOHAB Process Cruise suggested absorption values of approximately 0.4 m^{-1} (in line with the simulated results) was found at salinities of ~33 in this region (data not shown). These salinities were recorded in the near-bottom waters at the EC-6 mooring located off the mouth of Charlotte Harbor in November (University of South Florida Coastal

Ocean Monitoring and Prediction System, 2004). Modeled results were reasonably accurate in replicating the observed cross-shelf gradient in IOPs present on the WFS (modeled results were within one standard deviation of the mean of the SeaWiFS estimates for the entire region).

On November 8th, simulated chlorophyll concentrations closely correlated with the satellite imagery. However, an interesting result was that the simulated backscattering estimate was far less on November 8th than estimated from the satellite imagery. Since backscattering in this model was driven by chlorophyll concentrations, this result suggests that a large fraction of the total backscattering in the nearshore environment is driven by particulate matter other than phytoplankton. Since this event occurred just after the landfall of Tropical Storm Mitch, it is reasonable to assume that there was a large amount of sediment in the shallow waters. These shallows were much closer to the satellite lines near Charlotte Harbor than to the north near Tampa Bay, possibly accounting for the large differences observed between the Charlotte Harbor and the entire domain estimates. The resuspended sediments may have also been delivered from inside Charlotte Harbor, as there were increased fresh water fluxes during this period. This result clearly suggests that sediment resuspension can substantially contribute to the IOPs following high-energy events and should be carried as an additional state variable in this model.

The nearshore-simulated absorption and chlorophyll on November 8th were higher than the one standard deviation lines of the nearshore satellite data and were likely a result of the physical forcing of the model (Fig. 8). During the months of September and October, downwelling conditions prevailed on the WFS as well as in the simulation. Downwelling conditions generated a situation whereby the simulated pulse event, released at the end of September, was driven downward and offshore (data not shown). The simulated detritus and CDM absorption results in November were impacted by the simulated downwelling conditions that prevailed during the month of October that drove this early pulse downward and offshore. When the simulated winds reversed direction at the end of October/beginning of November, the colored matter from the DOY 267 pulse was carried upwards and onshore at nearly the same time as the second pulse event on November 5th (DOY 309). The

additive effect of these two occurrences led to a collection of detrital matter and CDM nearshore in shallow waters, resulting in an overestimation of simulated absorption on November 8th.

In spite of these higher nearshore simulated results, it is clear that the CDM pool in Case 1 is not sufficient to replicate the concentrations observed nearshore. However, when terrestrial CDM and nutrients were available at the shoreward boundary in the Case 2 study, the observed phytoplankton biomass as well as the vertical structure of the IOPs, is more robustly reproduced. The riverine-derived colored organic matter associated with freshwater discharges from the Peace and Caloosahatchee Rivers have also been shown to have a considerable impact on the absorption of the surrounding coastal waters (Del Castillo et al., 2001). Its inclusion as a separate state variable allows for the direct modeling of a simulated terrestrial nutrient and color addition providing a data set with which to confirm both the physical and ecological model.

On the WFS, the chromophoric compounds in DOM play a vital role in the surface waters by strongly absorbing UV radiation. Upon the absorption of sunlight, this CDOM can undergo a series of chemical reactions (photodegradation) yielding labile DOM, which can be rapidly assimilated by bacteria stimulating bacterial reproduction and regeneration of nutrients, which in turn may stimulate the production of phytoplankton (Bissett, 1997; Bissett et al., 1999b). In this simulation, changes in the labile-colored dissolved organic carbon ($CDOC_1$) pool were driven by the photochemical destruction of colored organic matter and by the supply via lysis and grazing of phytoplankton and bacteria. At first brush, the impacts of the photochemical destruction cycle on total IOP distributions appear to be limited. However, this result was mainly because most of the CDM losses were via advection out of the domain of the model. This may suggest that mixing of terrestrial waters on the shelf may be an important supply of color beyond the 40-m isobath. A more complete 4D solution over the larger domain of the WFS would require that these loss processes be included to match the spatial and temporal evolution of the CDM signal. The explicit inclusion of CDOM concentrations, including terrestrial supplies, and the in situ biochemical production cycle were required to match IOP distribution on the WFS.

The delivery of terrestrial material via rivers is a potentially large source of allocthonous nutrients (inorganic and organic) capable of greatly influencing primary productivity and total ocean color in local coastal regions, and CDOM appears to be a viable marker for tracking color and terrestrial nutrient sources from the land to coastal communities. The WFS is characterized by high salinities and low CDOM, making it an excellent candidate to evaluate the effects of terrestrial CDOM on the nearshore environment. It has been shown that the West Florida Shelf is greatly influenced by the input of CDOM from river sources during strong freshwater pulse events (Del Castillo et al., 2001). Carbon from terrestrial sources, via rivers, is a major component of the global carbon cycle. It has been estimated that approximately 40% of the 1 Gt of carbon flux is accounted for by organic carbon (Degens et al., 1991; Meybeck, 1993; Probst et al., 1994). In this model, the dissolved organic carbon (DOC) flux simulated at the nearshore boundary is estimated, based on nutrient concentrations in Charlotte Harbor and the adjacent rivers, to be approximately 397 µM DOC on the pulse day. This is 81% of the DOC concentration found in the lower Mississippi River, which has been estimated to be 489 µM DOC (Bianchi et al., 2004). While the magnitude of discharge flushed out onto the WFS is small compared to the Mississippi (only 3.5% that of the average discharge from the lower Mississippi River; Bianchi et al., 2004), the area surrounding Charlotte Harbor is commensurately smaller, and this is a significant amount of organic matter released to this small area. The results presented here demonstrate that significant riverine organic carbon fluxes released to the WFS have the potential for powerful ecological effects, including a dramatic increase in dissolved color as simulated by the increase in CDM absorption at the shoreward boundary (in November, the pulse case compared to the no-pulse case) as well as the establishment of high chlorophyll concentrations nearshore directly following a terrestrial nutrient addition. The exclusion of these terrestrial impacts from a simulation experiment of phytoplankton production would thus appear to be of limited value to the ecological understanding of this region of the WFS.

The ability to track CDOM from terrestrial sources to the ocean is also of concern in the

global carbon cycle. This model allows for the tracking of allochthonous as well as autochthonous CDOM sources. The use of biooptics to track terrestrial water sources is not a new concept. In the past, it has been used to determine the amount of terrestrial CDOM discharged by the Orinoco River and the impacts of this color constituent on the Caribbean during high flow conditions (Blough et al., 1993; Müller-Karger and Varela, 1990; Müller-Karger and Castro, 1994; Müller-Karger et al., 1989). The impacts from the Mississippi River are shown in this volume (Chen et al., 2004). In the Neuse River Estuary in North Carolina, periods of high flow, rainfall, and runoff, such as after Hurricane Fran, were associated with enrichment of the estuary by organic matter (Paerl et al., 1998). The optical properties of river CDOM provide the advantage of allowing for the monitoring and tracking of the surface circulation of freshwater from river runoff in the St. Lawrence Estuary in Canada (Nieke et al., 1997). These are but a few of the examples where the color from terrestrial CDOM has been used to illuminate the importance of terrestrial/coastal ocean interactions.

The results seem to confirm that, on the whole, the West Florida Shelf is a light-rich, nutrient-poor regime, i.e., light-saturated primary producers, and the decrease in total spectral photon densities of 1.5% in the Case 0-Photo was not matched by the 0.2% decrease in primary production. A truer measure of light saturation would be to incorporate the average photosynthetic action spectra into this calculation. However, the reduction in 0-Photo spectral light is in the blue end of the spectrum, as CDM absorption peaks in the visible at 400 nm. Thus, the removal of photons resulting from an increase in CDM concentration in the 0-Photo case would have expected to be blue-rich, making this a conservative estimate of average light saturation.

In this study, CDOM is used as both a tool to help track and estimate terrestrial fluxes as well as a diagnostic variable to test internal ecological interactions. These results demonstrate the importance of accurately modeling the optical components of the water column (Case 1 vs. Case 2 results) so as to shed light on the importance of CDOM in the prediction and monitoring of rivers as terrestrial nutrient sources in the nearshore environment.

Along with these predictions, this model also demonstrates that, on the WFS, refinements to the ecological and biogeochemical components are also necessary (e.g., non-Redfield stoichiometry, photoadaption, and various phytoplankton species) to accurately hindcast or forecast the ecological state of the WFS. This paper is the first of many small steps to address the larger goals of integrated 4D changes in coastal ocean color and biogeochemistry.

6. Summary

This biophysical model attempts to represent the ecological state of the water on the WFS in column in the summer and fall of 1998. This model accounts for phytoplankton competition, bacterial processes, DOM and CDOM cycling, particulate and dissolved organic regeneration, and the cycling of optical properties on the West Florida Shelf. The explicit use of Inherent Optical Properties allows us to directly compare the results of the simulations to ocean color remote sensing products. The model and simulation results provide a good basis from which to expand our use of remote sensing as a means of estimating and predicting the ecological dynamics of the coastal zone.

The strong nearshore to offshore color gradients do not appear to be driven by Loop Current intrusions into the nearshore environment; however, this result is tempered by the use of a 2D simulation. The Case 1 simulation results, which have no terrestrial influences, were generally all below the mean of the satellite-estimated CDOM absorption and frequently below the threshold of one standard deviation. Results from this model suggest that the terrestrial influx of color and nutrients, represented by the Case 2 example, must be included in any simulation of color and ecology within the 40-m isobath on the WFS. This strongly suggests that efforts to predict the color and clarity of the water column require the accurate resolution of fresh water fluxes and the concomitant inorganic and organic nutrient and color constituents. In addition, it also suggests that biogeochemical cycling, i.e., carbon cycling, may require the resolution of variable stoichiometries of carbon and nutrients supply, uptake, and regeneration in

order to predict carbon fluxes in the coastal zone. If these results hold for larger 4D simulations, ecological models that seek to forecast important ecological events, i.e., Harmful Algal Blooms, will be required to incorporate terrestrial fluxes as well as the nonstoichiometric relationship between nutrients and color.

Acknowledgements

Table A.2
Phytoplankton functional groups

Group number	Species type	References
FG 1	Prochlorococcus (high chl b)	(Moore et al., 1995; Partensky et al., 1993)
FG 2	Prochlorococcus (low chl b)	(Moore et al., 1995; Partensky et al., 1993)
FG 3	Synechococcus	(Barlow and Alberte, 1985; Glibert and Ray, 1990; Kana et al., 1992; Kana and Glibert, 1987; Moore et al., 1995)
FG 4	Generic large diatom	(Cleveland and Perry, 1987; Geider and Osborne, 1987; Geider and Platt, 1986; Haxo, 1985; Hoepffner and Sathyendranath, 1992; Jeffrey, 1976; Laws and Bannister, 1980; Perry et al., 1981; Schofield et al., 1990)
FG 5	Generic small diatom (<5 μm diameter)	(Geider et al., 1985; Reynolds et al., 1997)
FG 6	Toxic dinoflagellate (cum Karenia brevis)	(Johnsen and Sakshaug, 1993; Shanley and Vargo, 1993)
FG 7	Generic nontoxic dinoflagellate	

Appendix A. Initial conditions and ecological parameters

The ecological model was initialized with constant concentrations over the domain (Table A.1). The total phytoplankton concentration was equally divided among the seven functional groups (Table A.2) and their C/χ ratios used to establish the other elemental state variables were given by the minimum levels for each functional group found in the functional group parameters table (Table A.3), where χ represents nitrogen, silica (where applicable), phosphorus, and iron. The initial C/χ ratios for bacteria were 5:60:1000 for nitrogen, phosphorus, and iron, respectively. The initial C/χ ratios for fecal matter were 8:8:128:1000 for nitrogen, silica, phosphorus, and iron, respectively. The initial C/χ ratios for DOC1 were 6.625:106 for nitrogen and phosphorus, respectively. The initial $C:\chi$ ratios for

Table A.1
Initial conditions

State variable	Concentration (μmol liter^{-1})
Total phytoplankton carbon	0.84
Total bacterial carbon	0.85
Fecal carbon 1	0.002
Fecal carbon 1	0.002
Dissolved organic carbon 1	2.75
Dissolved organic carbon 2	55.0
Colored dissolved organic carbon 1	0.636
Colored dissolved organic carbon 2	0.057
Nitrate	0.25
Ammonia	0.025
Silicate	0.25
Phosphate	0.0172
Iron	0.001

Table A.3
Phytoplankton parameter values

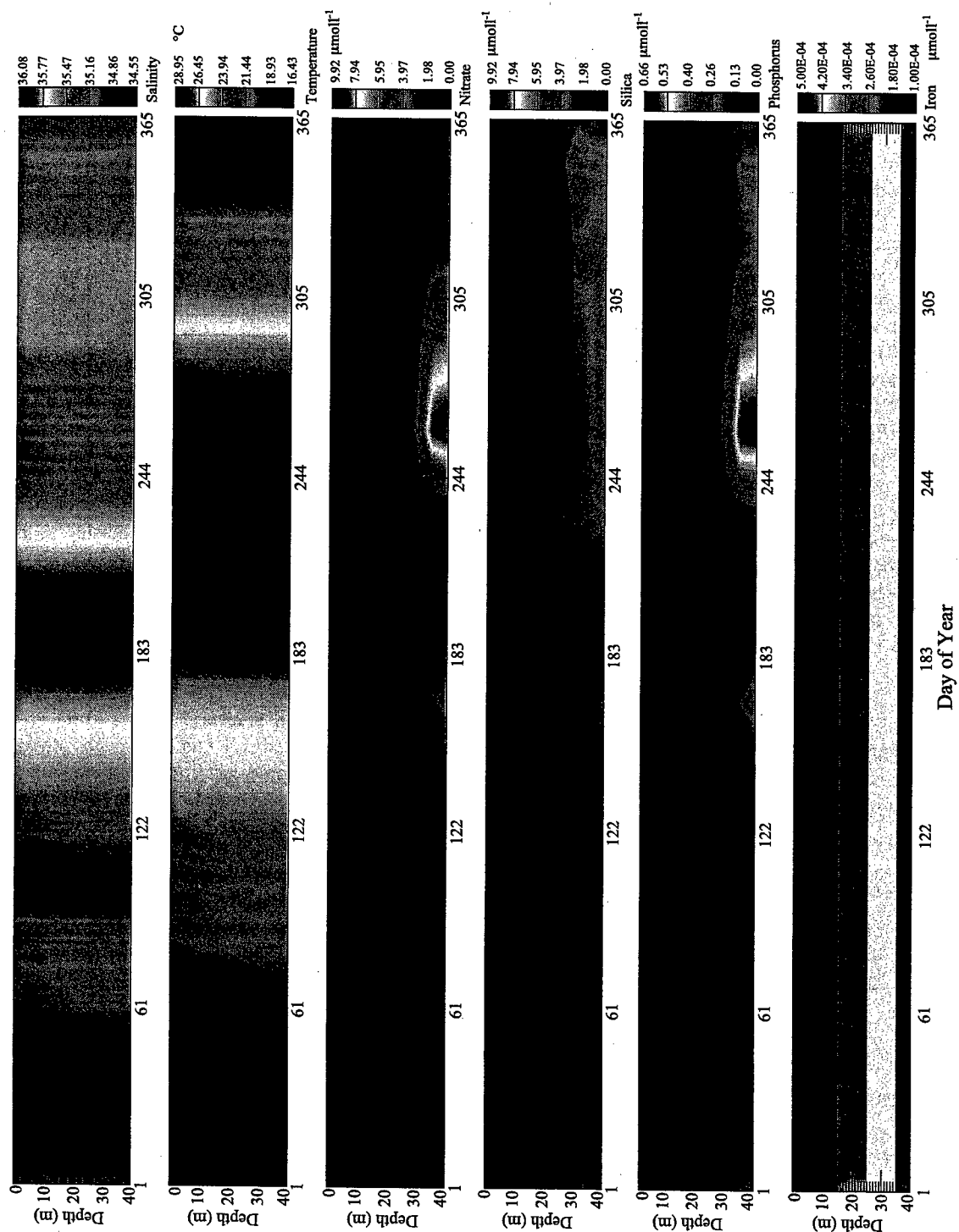|	FG 1	FG 2	FG 3	FG 4	FG 5	FG 6	FG 7
μm	1.28	1.45	2.00	3.70	3.70	1.00	2.00
K_{sNO3}	0.100	0.100	0.167	0.824	0.412	0.824	0.824
K_{sNH4}	0.050	0.050	0.083	0.414	0.208	0.414	0.414
K_{sSiO}	N/A	N/A	N/A	1.824	1.412	N/A	N/A
K_{sPO4}	0.00625	0.00625	0.01044	0.05150	0.02575	0.05150	0.05150
K_{sFe}	N/A	N/A	N/A	N/A	N/A	N/A	N/A
K_{sDON}	N/A	N/A	N/A	N/A	N/A	2.0	2.0
K_{sDOP}	N/A	N/A	N/A	N/A	N/A	2.0	2.0
ψ	12.00	12.00	6.50	1.28	2.60	1.28	1.28
Max C:N	6.625	6.625	6.625	14.000	17.750	17.000	17.000
Min C:N	6.625	6.625	6.625	6.625	6.625	6.625	6.625
Max C:Si	N/A	N/A	N/A	5.521	5.521	N/A	N/A
Min C:Si	N/A	N/A	N/A	5.521	5.521	N/A	N/A
Max C:P	106.0	106.0	106.0	106.0	106.0	130.0	130.0
Min C:P	106.0	106.0	106.0	106.0	106.0	106.0	106.0
Max C:Fe	N/A	N/A	N/A	N/A	N/A	N/A	N/A
Min C:Fe	N/A	N/A	N/A	N/A	N/A	N/A	N/A
K_{sDON} C:N	N/A	N/A	N/A	N/A	N/A	14.0	14.0
K_{sDOP} C:P	N/A	N/A	N/A	N/A	N/A	110.0	110.0
ϕ_m	0.0833	0.0833	0.0833	0.0833	0.0833	0.0833	0.0833
E_{0_comp}	1.0	6.0	6.0	10.0	10.0	10.0	10.0
$E_{0\_inhibit}$	40.0	105.0	10000.0	10000.0	10000.0	10000.0	10000.0
Decay rate	0.100	0.001	0.000	0.000	0.000	0.000	0.000
θ_{n_max}	100.0	150.0	160.0	60.0	42.0	124.0	124.0
Slope$_{\theta ll}$	0.8000	0.3000	0.1000	0.1200	0.1144	0.4779	0.4779
θ_{0ll}	20.00	15.00	30.00	25.00	14.80	47.53	47.53
Slope$_{\theta nl}$	N/A	N/A	N/A	12.20	6.832	10.35	10.35
θ_{0nl}	N/A	N/A	N/A	60.0	42.0	124.0	124.0
Slope$_{PacEff}$	N/A	N/A	N/A	0.01429	0.01838	N/A	N/A
Max$_{PacEff}$	N/A	N/A	N/A	0.50000	0.50000	N/A	N/A
Slope$_{\zeta ChlB}$	−0.02	−0.00100	N/A	N/A	N/A	N/A	N/A
ζ_{ChlB}	2.4	0.2	N/A	N/A	N/A	N/A	N/A
Slope$_{\zeta ChlC}$	N/A	N/A	N/A	−0.00136	−0.00120	0.00000	0.00000
ζ_{ChlC}	N/A	N/A	N/A	0.340	0.340	0.056	0.056
Slope$_{\zeta PSC}$	N/A	N/A	N/A	−0.012	−0.0104	0.0000	0.0000
ζ_{PSC}	N/A	N/A	N/A	2.000	2.000	1.106	1.106
Slope$_{\zeta PPC}$	0.0138	0.0162	0.0090	0.0000	0.0000	0.0018	0.0018
ζ_{PPC}	0.3000	0.3000	0.3000	0.1000	0.1000	0.1600	0.1600
slope$_{\zeta LPUb}$	N/A	N/A	N/A	N/A	N/A	N/A	N/A
ζ_{LPUb}	N/A	N/A	N/A	N/A	N/A	N/A	N/A
Slope$_{\zeta HPUb}$	N/A	N/A	−0.1300	N/A	N/A	N/A	N/A
ζ_{HPUb}	N/A	N/A	20.000	N/A	N/A	N/A	N/A
FecDOC	0.41670	0.41670	0.41670	0.33330	0.33330	0.33330	0.33330
FecPEL(1)	0.08335	0.08335	0.08335	0.16670	0.16670	0.16670	0.16670
FecPEL(2)	0.08335	0.08335	0.08335	0.16670	0.16670	0.16670	0.16670
FecCYC	0.41660	0.41660	0.41660	0.33330	0.33330	0.33330	0.33330
e	0.005	0.005	0.005	0.005	0.005	0.005	0.005
w_S	0.0	0.0	0.0	0.0	0.0	0.0	0.0
Mortality	0.01	0.01	0.01	0.01	0.01	0.01	0.01
Refuge	0.02	0.02	0.02	0.02	0.02	0.02	0.02

Fig. A.1. The offshore boundary conditions for EcoSim Case 1 and Case 2, top 40 m of the water column, displaying (a) salinity, (b) temperature, (c) nitrate, (d) silica, (e) phosphorus, and (f) iron inputs on the WFS. The gulf-side boundary conditions change seasonally and are derived from the 1998/1999 ECOHAB cruises on the WFS (data not shown).

DOC2 were 15:106 for nitrogen and phosphorus, respectively. Temporal offshore boundary conditions can be seen in Fig. A.1. The shoreward boundary conditions used on DOY 267 and 309 are in Table A.5. Parameters not listed in Tables A.1–A.5 are given in Bissett et al., 1999a,b.

Appendix B. Physical circulation model

B.1. Physical Model

The earlier work of Mellor (1998), Hamilton and Rattray (1978), and Leendertse et al. (1973) were instructive in constructing the physical model. A modified Bott's positive-definite numerical advection scheme (Easter, 1993) is used and the cross-shelf

Table A.4
Other state variable parameter values

State variable	Value
Bacterial	
μ_{m_b}	2.0
Bac C:N	5:1
Bac C:P	12:1
Bac C:Fe	1000:1
K_{s_BDOCl}	130.0
K_{s_BNH4}	26.0
K_{s_BDIP}	10.833
K_{s_BDIFe}	2.6
GGE_c	0.300
GGE_X	1.000
e_{bc}	0.040
e_{bn}	0.005
Maximum 24 h AtoN	0.040
K_{sNit}	0.100
w_{sb}	0.000
*Bac*DOC	0.4583
*Bac*PEL(1)	0.0834
*Bac*PEL(2)	0.0000
*Bac*CYC	0.4583
Fecal	
w_{sF1}	0.00
w_{sF2}	Infinite
Dissolved organic matter	
*color*FR$_1$	0.0323
*color*FR$_2$	0.0930
*Rt*UVDOC	0.0034
*Rt*UVDIC	0.0193
$a*CDOC_1$	5.080
$a*CDOC_2$	5.080
S_{UV}	0.0145

Table A.5
Inshore boundary conditions for pulse case. Concentrations were added to state variables on DOY 267 and 309

State variable	Concentration (μmol liter^{-1})
Dissolved organic carbon 1	397.263
Dissolved organic nitrogen 1	20.054
Dissolved organic phosphorus 1	1.3
Colored dissolved organic carbon 1	0.82
Colored dissolved organic carbon 2	8.2
Nitrate	0.947
Ammonia	1.309
Silicate	9.46
Phosphate	0.867
Iron	0.003

density gradient is a prescribed term independent of depth and the offshore coordinate. The physical model is formulated as a diagnostic model, and the velocity field is forced to adjust to the prescribed density field. The hydrostatic and Boussinesq approximations are invoked. Linear dynamics are assumed outside of the nonlinear bottom stress formulation.

Assuming that all alongshore gradients may be neglected, and ignoring nonlinear advection processes, the governing equations are:

$$\frac{\partial u}{\partial t} - fv = \frac{g}{\rho_o} \int_z^\eta \frac{\partial \rho}{\partial x} dz - g \frac{\partial \eta}{\partial x}$$

$$+ \frac{\partial}{\partial z} K_M \frac{\partial u}{\partial z} + K_X \frac{\partial^2 u}{\partial x^2} \tag{B.1}$$

$$\frac{\partial v}{\partial t} + fu = \frac{\partial}{\partial z} K_M \frac{\partial v}{\partial z} + K_X \frac{\partial^2 v}{\partial x^2} \tag{B.2}$$

$$\frac{\partial w}{\partial z} + \frac{\partial u}{\partial x} = 0 \tag{B.3}$$

$$\frac{\partial \eta}{\partial t} = -\frac{\partial}{\partial x} \int_{-h}^\eta u \, dz \tag{B.4}$$

where: x, y, z: Cartesian coordinates with x positive offshore, y positive down coast and z positive upward; t: time; u, v, w: velocity components in the x, y, z directions, respectively; η: sea surface elevation, ρ: density, ρ_o: reference density(1023.0 kg m^{-3}); f: Coriolis parameter (6.47×10^{-5} s^{-1}); g: gravity(9.81 m^2 s^{-1}); K_M: vertical turbulent eddy viscosity(10 cm^2

s^{-1}); K_X: horizontal turbulent eddy viscosity(1×10^4 cm^2 s^{-1}); h: depth of the water column relative to mean sea level.

The equation for the sea surface elevation, 0, is derived from the surface boundary condition on w in Eq. (B.3) and is given by Eq. (B.4).

$$K_M \left(\frac{\partial u}{\partial z}, \frac{\partial v}{\partial z} \right)_{z=\eta} = \left(\frac{\tau_x}{\rho_o}, \frac{\tau_y}{\rho_o} \right) \qquad (B.5)$$

$$(\tau_x, \tau_y) = \rho_a C_s \left(U_s^2 + V_s^2 \right)^{1/2} (U_s, V_s) \qquad (B.6)$$

$$C_s = 0.934 \times 10^{-3} + 0.788 \times 10^{-4} \left(U_s^2 + V_s^2 \right)^{1/2}$$
$$\qquad - 0.616 \times 10^{-6} \left(U_s^2 + V_s^2 \right) \qquad (B.7)$$

$$K_M \left(\frac{\partial u}{\partial z}, \frac{\partial v}{\partial z} \right)_{z=-h} = C_d(u_b^2 + v_b^2)(u_b, v_b) = 0.0025 \qquad (B.8)$$

$$\eta = \hat{u} / (gh)^{1/2} \qquad (B.9)$$

The vertical boundary condition at the surface in Eqs. (B.1) and (B.2) is given by Eq. (B.5). The wind stress components, τ_x, and τ_y, are calculated from Eqs. (B.6) and (B.7), where $\rho_a = 1.255$ kg m^{-3} is the density of air, U_s, and V_s, the cross-shelf and along-shelf components of the wind, respectively, and the surface drag coefficient, C_s, is from Hellerman and Rosenstein (1983) ignoring air–sea temperature differences.

The boundary condition at the bottom of the water column is given by Eq. (B.8), where u_b and v_b are the velocity components in the bottom most layer of the water column. Momentum is lost through bottom friction and also through lateral friction along solid boundaries where the normal or u component is set to zero and a no slip condition is prescribed for the tangential or v component of the flow.

Following Hamilton and Rattray (1978), the condition at the open offshore boundary is given by equation B.9, where $\hat{u}$ is the depth averaged flow adjacent to the boundary. This condition permits surface gravity waves to propagate out of the domain without reflection. For the lateral friction terms, a slip condition is prescribed on the tangential component of

the flow, and the eddy flux of momentum of the component normal to the boundary is set to zero.

B.2. Numerical methods

The cross-shelf transect for the physical model extended 170 km offshore to the 150-m isobath. A minimum depth of 10 m was prescribed at the coast. The vertical increment of the finite difference grid, Δz, was 1 m, and the horizontal increment, Δx, was 1 km. With a fixed Δz, the number of active layers varied with the bottom depth, giving the bottom topography a staircase representation. The finite difference grid was staggered, with η at cell centers, u and v at cell interfaces $\pm \Delta x / 2$ from cell centers, and w at cell interfaces $\pm \Delta z / 2$ from cell centers.

The centered leapfrog technique was used to step forward in time with the diffusion terms lagged one time step for computational stability. A time filter (Asselin, 1972) was used to prevent decoupling of the solution at odd and even time steps. Spatial gradients were approximated by centered differences. A time step of 10 s was used, dictated by the CFL condition (Roach, 1976), based on the speed of surface gravity waves.

B.3. Model runs

The physical model was used to calculate quasi-steady monthly flow fields. This was accomplished

Table B.1
Resultant wind stress magnitude in Pascals ($\times 10^{-2}$), wind stress direction in degrees from true north, and cross-shelf density gradient (kg m$^{-4} \times 10^{-5}$)

| | Wind stress | | Density |
	Magnitude	Direction	Gradient
January	0.1	359	0.9
February	0.9	289	0.5
March	0.3	350	1.3
April	1.3	237	1.4
May	1.9	263	1.3
June	1.9	276	1.3
July	0.9	274	1.2
August	0.1	354	0.7
September	0.9	150	1.1
October	0.6	038	0.7
November	0.3	029	−0.03
December	0.6	027	0.0

by stepping the model equations forward in time for 720 h of simulated time, holding the wind stress and density constant. Monthly resultant wind stress components were calculated using hourly or 3-hourly wind data from Tampa International Airport. The density field was input as a constant cross-shelf gradient, independent of depth or distance offshore. These gradients were derived from cross-shelf averages of depth-averaged densities from 1998/1999 hydrographic data on the West Florida shelf. The monthly values for the wind stress and density gradients are given in Table B.1.

For the biological model calculations, the two dimensional velocity components, u and w, were interpolated at each time step from corresponding quasi-steady monthly fields. Steady, mass conservative flow fields were obtained by adjusting the interpolated u field using Eq. (B.3), progressing from the coast where $u=0$ to the 40 m isobath and forcing $w=0$ at the sea surface.

References

Arnone, R.A., Martinolich, P., Gould Jr., R.W., Stumpf, R., Ladner, S., 1998. Coastal optical properties using SeaWiFS. Ocean Optics vol. XIV. SPIE, the International Society for Optical Engineering, Kailua-Kona Hawaii.

Asselin, R., 1972. Frequency filters for time integration. Monthly Weather Review 100, 487–490.

Banse, K., 1995. Zooplankton: pivotal role in the control of ocean production. ICES Journal of Marine Science 52, 265–277.

Barlow, R.G., Alberte, R.S., 1985. Photosynthetic characteristics of phycoerythrin-containing marine *Synechococcus* spp. Marine Biology 86, 63–74.

Bianchi, T.S., Filley, T., Dria, K., Hatcher, P.G., 2004. Temporal variabilty in sources of dissolved organic carbon in the lower Mississippi River. Geochimica et Cosmochimica Acta 68 (5), 959–967.

Bissett, W.P., 1997. Carbon cycling in the upper waters of the Sargasso Sea. Dissertation Thesis. University of South Florida, St. Petersburg, 207 pp.

Bissett, W.P., Meyers, M.B., Walsh, J.J., Muller-Karger, F.E., 1994. The effects of temporal variability of mixed layer depth on primary productivity around Bermuda. Journal of Geophysical Research 99 (C4), 7539–7553.

Bissett, W.P., Patch, J.S., Carder, K.L., Lee, Z., 1997. Pigment packaging and chlorophyll *a*-specific absorption in high-light oceanic waters. Limnology and Oceanography 42 (5), 961–968.

Bissett, W.P., Carder, K.L., Walsh, J.J., Dieterle, D.A., 1999a. Carbon cycling in the upper waters of the Sargasso Sea: II. Numerical simulation of apparent and inherent optical proper-

ties. Deep-Sea Research, Part I: Oceanographic Research Papers 46 (2), 271–317.

Bissett, W.P., Walsh, J.J., Dieterle, D.A., Carder, K.L., 1999b. Carbon cycling in the upper waters of the Sargasso Sea: I. Numerical simulation of differential carbon and nitrogen fluxes. Deep-Sea Research, Part I: Oceanographic Research Papers 46 (2), 205–269.

Bissett, W.P., Schofield, O., Glenn, S., Cullen, J.J., Miller, W.L., Plueddemann, A.J., Mobley, C.D., 2001. Resolving the impacts and feedback of ocean optics on upper ocean ecology. Oceanography 14 (3), 30–53.

Bissett, W.P., Arnone, R., DeBra, S., Dye, D., Kirkpatrick, G., Mobley, C., Schofield, O.M., 2003. The integration of ocean color remote sensing with coastal nowcast/forecast simulations of harmful algal blooms (HABs) (In preparation).

Bissett, P., Arnone, R., DeBra, S., Dye, D., Kirkpatrick, G., Mobley, C., Schofield, O.M., 2004a. Predicting apparent optical properties on the West Florida Shelf: the coupling of inherent optical properties to a robust radiative transfer model (In preparation).

Bissett, W.P., DeBra, S., Dye, D., 2004b. Ecological Simulation (EcoSim) 2.0 Technical Description. Florida Environmental Research Institute, Tampa. http://www.flenvironmental.org/publications_ppts/FERI_2004_0002_U_D.pdf.

Blough, N.V., Zafiriou, O.C., Bonilla, J., 1993. Optical absorption spectra of waters from the Orinoco River outflow: terrestrial input of colored organic matter to the Caribbean. Journal of Geophysical Research 98 (C2), 2271–2278.

Bogdanov, D.V., Sokolov, V.A., Khromov, N.S., 1967. Regions of high biological and commercial productivity in the Gulf of Mexico and Caribbean Sea. Oceanology 8 (3), 371–381.

Carder, K.L., Steward, R.G., 1985. A remote-sensing reflectance model of a red-tide dinoflagellate off west Florida. Limnology and Oceanography 30, 286–298.

Carder, K.L., Steward, R.G., Harvey, G.R., Ortner, P.B., 1989. Marine humic and fulvic acids: their effects on remote sensing of ocean chlorophyll. Limnology and Oceanography 34 (1), 68–81.

Carder, K.L., Chen, F.R., Lee, Z.P., Hawes, S.K., Kamykowski, D., 1999. Semianalytic Moderate-Resolution Imaging Spectometer algorithms for chlorophyll a and absorption with bio-optical domains based on nitrate-depletion temperatures. Journal of Geophysical Research 104 (C3), 5403–5421.

Carlson, C.A., 2002. Production and removal processes. In: Hansell, D.A., Carlson, C.A. (Eds.), Biogeochemistry of Marine Dissolved Organic Matter. Academic Press, Amsterdam, pp. 91–151.

Carlson, C.A., Ducklow, H.W., 1996. Growth of bacterioplankton and consumption of dissolved organic carbon in the oligotrophic Sargasso Sea. Aquatic Microbial Ecology 10, 69–85.

Carlson, C.A., Ducklow, H.W., Sleeter, T.D., 1996. Stocks and dynamics of bacterioplankton in the northwestern Sargasso Sea. Deep-Sea Research, Part II: Topical Studies in Oceanography 43 (1–2), 491–516.

Chen, F.R., Bissett, W.P., Coble, P., Conmy, R.G., Gardner, B., Moran, M.A., Wang, X., Wells, M.L., Whelan, P., Zepp, R.G., 2004. Chromophoric Dissolved Organic Matter (CDOM) source

characterization in the Louisiana Bight. Marine Chemistry 89 (1–4), 257–272.

Clark, L.L., Ingall, E.D., Benner, R., 1998. Marine phosphorus is selectively remineralized. Nature 393 (6684), 426.

Cleveland, J.S., Perry, M.J., 1987. Quantum yield, relative specific absorption and fluorescence in nitrogen-limited *Chaetoceros gracilis*. Marine Biology 94, 489–497.

Degens, E.T., Kempe, S., Richey, J.E., 1991. Summary: biogeochemistry of major world rivers. In: Degens, E.T., Kempe, S., Richey, J.E. (Eds.), Biogeochemistry of Major World Rivers SCOPE Rep vol. 42. John Wiley, New York, pp. 323–347.

Del Castillo, C.E., Coble, P.G., 2000. Seasonal variability of the colored dissolved organic matter during the 1994–95 NE and SW monsoons in the Arabian Sea. Deep-Sea Research, Part II: Topical Studies in Oceanography 47 (7–8), 1563–1579.

Del Castillo, C.E., Gilbes, F., Coble, P.B., Muller-Karger, F.E., 2000. On the dispersal of riverine colored dissolved organic matter over the West Florida Shelf. Limnology and Oceanography 45 (6), 1425–1432.

Del Castillo, C.E., Coble, P.G., Conmy, R.N., Mueller-Karger, F.E., Vanderbloemen, L., Vargo, G.A., 2001. Multispectral in situ measurements of organic matter and chlorophyll fluorescence in seawater: documenting the intrusion of the Mississippi River plume in the West Florida Shelf. Limnology and Oceanography 46 (7), 1836–1843.

Dragovich, A., Kelly, J.A., Goodell, G., 1968. Hydrological and biological characteristics of Florida's West Coast Tributaries. Fishery Bulletin 66 (3), 463–477.

Easter, R.C., 1993. Two modified versions of Bott's positive-definite numerical advection scheme. Monthly Weather Review 121, 297–305.

Florida Fish and Wildlife Conservation Commission and Florida Marine Research Institute–ECOHAB Cruise Data, 2004. http://www.floridamarine.org/features/view_article.asp?id=8820%20#25324.

Florida Fish and Wildlife Conservation Commission and Florida Marine Research Institute (FMRI). Red Tides in Florida, 1954–1998: Harmful Algal Bloom Historical Database.

Geider, R.J., Osborne, B.A., 1987. Light absorption by a marine diatom: experimental observations and theoretical calculations of the package effect in a small *Thalassiosira* species. Marine Biology 96, 299–308.

Geider, R.J., Platt, T., 1986. A mechanistic model of photoadaptation in microalgae. Marine Ecology. Progress Series 30, 85–92.

Geider, R.J., Osborne, B.A., Raven, J.A., 1985. Light dependence of growth and photosynthesis in *Phaeodactylum tricornutum* (Bacillariophyceae). Journal of Phycology 21, 609–619.

Gilbes, F., Tomas, C., Walsh, J.J., Muller-Karger, F.E., 1996. An episodic chlorophyll plume on the West Florida Shelf. Continental Shelf Research 16 (9), 1201–1224.

Glibert, P.M., Ray, R.T., 1990. Different patterns of growth and nitrogen uptake in two clones of marine *Synechococcus* spp. Marine Biology 107, 273–280.

Goldman, J.C., Caron, D.A., Dennett, M.R., 1987. Regulation of gross growth efficiency and ammonium regeneration in bacteria by subtrate C:N ratio. Limnology and Oceanography 32 (6), 1239–1252.

Gordon, H., Wang, M., 1994. Retrieval of water leaving radiance and aerosol optical thickness over the ocean with SeaWiFS: a preliminary algorithm. Applied Optics 33 (3), 443–452.

Gordon, H.R., Clark, D.K., Brown, J.W., Brown, O.B., Evans, R.H., Broenkow, W.W., 1983. Phytoplankton pigment concentrations in the Middle Atlantic Bight: comparison of ship determinations and CZCS estimates. Applied Optics 22 (1), 20–36.

Gould, R.W., Arnone, R.A., 1998. Three-dimensional modelling of inherent optical properties in a coastal environment: coupling ocean colour imagery and in situ measurements. International Journal of Remote Sensing 19 (11), 2141–2159.

Gregg, W.W., Walsh, J.J., 1992. Simulation of the 1979 spring bloom in the Mid-Atlantic Bight: a coupled physical/biological/optical model. Journal of Geophysical Research 97 (C4), 5723–5743.

Hamilton, P., Rattray Jr., M., 1978. A numerical model of the depth-dependent, wind-driven upwelling circulation on a continental shelf. Journal of Physical Oceanography 8, 437–456.

Hansell, D.A., Carlson, C.A., 2002. Biogeochemistry of Marine Dissolved Organic Matter. Academic Press. 774 pp.

Haxo, F.T., 1985. Photosynthetic action spectrum of the coccolithophorid, *Emiliania huxleyi* (Haptophyceae): 19′ hexanoyloxyfucoxanthin as antenna pigment. Journal of Phycology 21, 282–287.

He, R., Weisberg, R., 2002a. West Florida Shelf circulation and temperature budget for the 1998 fall transition. Continental Shelf Research 23 (8), 777–800.

He, R., Weisberg, R., 2002b. West Florida Shelf circulation and temperature budget for the 1999 spring transition. Continental Shelf Research 22, 719–748.

Hellerman, S., Rosenstein, M., 1983. Normal monthly wind stress over the world ocean with error estimates. Journal of Physical Oceanography 13, 1093–1104.

Hoepffner, N., Sathyendranath, S., 1992. Bio-optical characteristics of coastal waters: absorption spectra of phytoplankton and pigment distribution in the western North Atlantic. Limnology and Oceanography 37 (8), 1660–1679.

http://www.nhc.noaa.gov/, National Weather Service Tropical Prediction Center National Hurricane Center, National Oceanic and Atmospheric Administration.

Jeffrey, S.W., 1976. The occurrence of chlorophyll C_1 and C_2 in algae. Journal of Phycology 12, 349–354.

Johnsen, G., Sakshaug, E., 1993. Bio-optical characteristics and photoadaptive responses in the toxic and bloom-forming dinoflagellates *Gyrodinum aurelum*, *Gymnodinium galatheanum*, and two strains of *Prorocentrum minimum*. Journal of Phycology 29, 627–642.

Kana, T.M., Glibert, P.M., 1987. Effect of irradiances up to 2000 $\mu E\ m^{-2}\ s^{-1}$ on marine *Synechococcus* WH7803-II. Photosynthetic responses and mechanisms. Deep-Sea Research 34 (4), 497–516.

Kana, T.M., Feiwel, N.L., Flynn, L.C., 1992. Nitrogen starvation in marine *Synechococcus* strains: clonal differences in phycobiliprotein breakdown and energy coupling. Marine Ecology. Progress Series 88, 75–82.

Kim, Y.S., Martin, D.F., 1974. Interrelationship of Peace River parameters as a basis of the iron index: a predictive guide to the Florida red tide. Water Research 8, 607–616.

Kirchman, D.L., Keil, R.G., Wheeler, P.A., 1989. The effect of amino acids on ammonium utilization and regeneration by heterotrophic bacteria in the subarctic Pacific. Deep-Sea Research 36 (11), 1763–1776.

Kirchman, D.L., Keil, R.G., Wheeler, P.A., 1990. Carbon limitation of ammonium uptake by heterotrophic bacteria in the subarctic Pacific. Limnology and Oceanography 35 (6), 1258–1266.

Laws, E.A., Bannister, T.T., 1980. Nutrient- and light-limited growth of *Thalassiosira fluviatilis* in continuous culture, with implications for phytoplankton growth in the ocean. Limnology and Oceanography 25 (3), 457–473.

Leendertse, J.J., Alexander, R.C., Liu, S.K., 1973. A three-dimensional model for estuaries and coastal seas. Principles of Computation vol. I. The Rand Corporation, Santa Monica, CA 90406.

Lenes, J.M., Darrow, B.P., Cattrall, C., Heil, C.A., Callahan, M., Vargo, G.A., Byrne, R.H., Prospero, J.M., Bates, D.E., Fanning, K.A., Walsh, J.J., 2001. Iron fertilization and the *Trichodesmium* response on the West Florida shelf. Limnology and Oceanography 46 (6), 1261–1277.

Mellor, G.L., 1998. Users Guide for A Three-dimensional Primitive Equation Numerical Ocean Model. Program in Atmospheric and Oceanic Sciences. Princeton University, Princeton, NJ 08544.

Meybeck, M., 1993. Riverine transport of atmospheric carbon: sources, global typology, and budget. Water, Air and Soil Pollution 70, 443–463.

Miller, W.L., Zepp, R.G., 1995. Photochemical production of dissolved inorganic carbon from terrestrial organic matter: significance to the oceanic organic carbon cycle. Geophysical Research Letters 22 (4), 417–420.

Mobley, C.D., 1994. Light and Water. Academic Press, San Diego, CA. 592 pp.

Mobley, C., Stramski, D., 1997. Effects of microbial particles on oceanic optics: methodology for radiative transfer modeling and example simulations. Limnology and Oceanography 42 (3), 550–560.

Moore, L.R., Goericke, R., Chisholm, S.W., 1995. Comparative physiology of *Synechococcus* and *Prochlorococcus*: influence of light and temperature on growth, pigments, fluorescence and absorptive properties. Marine Ecology. Progress Series 116, 259–275.

Moore, J.K., Doney, S.C., Glover, D.M., Fung, I.Y., 2001. Iron cycling and nutrient limitation patterns in surface waters of the World Ocean. Deep-Sea Research, Part II: Topical Studies in Oceanography 49 (1–3), 463–507.

Moran, M.A., Sheldon, W.M., Zepp, R.G., 2000. Carbon loss and optical property changes during long-term photochemical and biological degradation of estuarine dissolved organic matter. Limnology and Oceanography 45 (6), 1254–1264.

Mote Marine Laboratory ECOHAB Cruise Flow Through Surface Maps, 2004. http://www.mote.org/~pederson/98pro.phtml.

Mulholland, M.R., Floge, S., Carpenter, E.J., Capone, D.G., 2002. Phosphorus dynamics in cultures and natural populations of *Trichodesmium* spp. Marine Ecology. Progress Series 239, 45–55.

Müller-Karger, F.E., Castro, R.A., 1994. Mesoscale processes affecting phytoplankton abundance in the southern Caribbean Sea. Continental Shelf Research 14 (2/3), 199–221.

Müller-Karger, F., Varela, R.J., 1990. Influjo del Rio Orinoco en el Mar Caribe: observaciones con el CZCS desde el espacio. Memoria Contribution 186 (50), 361–390.

Müller-Karger, F.E., McClain, C.R., Fisher, T.R., Esaias, W.E., Varela, R., 1989. Pigment distribution in the Caribbean Sea: observations from space. Progress in Oceanography 23, 23–64.

Nelson, N.B., Siegel, D.A., Michaels, A.F., 1998. Seasonal dynamics of colored dissolved material in the Sargasso Sea. Deep-Sea Research 45 (6), 931–957.

Nieke, B., Reuter, R., Heuermann, R., Wang, H., Babin, M., Therriault, J.C., 1997. Light absorption and fluorescence properties of chromophoric dissolved organic matter (CDOM), in the St. Lawrence Estuary (Case 2 waters). Continental Shelf Research 17 (3), 235–252.

O'Brien, J.J., 1986. The diffusive problem. In: O'Brien, J.J. (Ed.), Advanced Physical Oceanographic Numerical Modelling. D. Reidel, Norwell, MA, pp. 127–144.

Ocean Circulation Group, 2004. http://ocg6.marine.usf.edu/shelf/Ecohab/EC61/, University of South Florida College of Marine Science.

O'Reilly, J.E., Maritorena, S., Mitchell, B.G., Siegel, D.A., Carder, K.L., Garver, S.A., Kahru, M., McClain, C., 1998. Ocean color chlorophyll algorithms for SeaWiFS. Journal of Geophysical Research 103, 24937–24953.

Paerl, H., Pickney, J., Fear, J., Peierls, B., 1998. Ecosystem responses to internal and watershed organic matter loading: consequences for hypoxia in the eutrophying Neuse River estuary, North Carolina, USA. Marine Ecology. Progress Series 166, 17–25.

Partensky, F., Hoepffner, N., Li, W.K.W., Ulloa, O., Vaulot, D., 1993. Photoacclimation of *Prochlorococcus* sp. (Prochlorophyta) strains isolated from the North Atlantic and the Mediterranean Sea. Plant Physiology 101, 285–296.

Perry, M.J., Talbot, M.C., Alberte, R.S., 1981. Photoadaption in marine phytoplankton: response of the photosynthetic unit. Marine Biology 62, 91–101.

Pond, S., Pickard, G.L., 1989. Introductory Dynamical Oceanography. Pergamon Press, New York. 329 pp.

Probst, J.L., Moratti, J., Tardy, Y., 1994. Carbon river fluxes and weathering CO2 consumption in the Congo and Amazon river basins. Applied Geochemistry 9, 1–13.

Reynolds, R.A., Stramski, D., Kiefer, D.A., 1997. The effect of nitrogen limitation on the absorption and scattering properties of the marine diatom *Thalassiosira pseudonana*. Limnology and Oceanography 42 (5), 881–892.

Riley, G.A., 1946. Factors controlling phytoplankton populations on Georges Bank. Journal of Marine Research 6, 114–125.

Roach, P.J., 1976. Computational Fluid Dynamics. Hermosa Publications, Albuquerque, New Mexico. 446 pp.

Rochell-Newall, E.J., Fisher, T.R., Fan, C., Gilbert, P.M., 1999. Dynamics of chromophoric dissolved organic matter and dissolved organic carbon in experimental mesocosms. Helgoland Marine Research 55 (1), 12–22.

Schofield, O., Bidigare, R.R., Prézelin, B.B., 1990. Spectral photosynthesis, quantum yield and blue-green light enhance-

ment of productivity rates in the diatom *Chaetoceros gracile* and the prymnesiophyte *Emiliania huxleyi*. Marine Ecology. Progress Series 64, 175–186.

Shanley, E., Vargo, G., 1993. Cellular Composition, Growth, Photosynthesis, and Respiration Rates of *Gymnodinium breve* Under Varying Light Levels. Toxic Phytoplankton Blooms in the Sea, pp. 831–836.

Siegel, D.A., Maritorena, S., Nelson, N.B., Hansell, D.A., Lorenzi-Kayser, M., 2002. Global distribution and dynamics of colored dissolved and detrital organic materials. Journal of Geophysical Research 107 (C12), 3228.

Steidinger, K.A., 2003. 1999–2002 ECOHAB Data. P. Bissett. Tampa/Saint Petersburg.

Steward, R., Haddad, K., Carder, K., 1978. Transmissometry on the West Florida–Alabama–Mississippi. Department of Marine Science University of South Florida, Tampa.

Stramski, D., Mobley, C., 1997. Effects of microbial particles on oceanic optics: a database of single-particle optical properties. Limnology and Oceanography 42 (3), 538–549.

Tester, P.A., Steidinger, K.A., 1997. *Gymnodinium breve* red tide blooms: initiation, transport, and consequences of surface circulation. Limnology and Oceanography 42 (5, part 2), 1039–1051.

Toole, D.A., Siegel, D.A., 2001. Modes and mechanisms of ocean color variability in the Santa Barbara Channel. Journal of Geophysical Research 111 (C106), 26985–27000.

University of South Florida Coastal Ocean Monitoring and Prediction System, 2004. http://comps.marine.usf.edu.

Vodacek, A., Blough, N.V., DeGrandpre, M.D., Peltzer, E.T., Nelson, R.K., 1997. Seasonal variation of CDOM and DOC in the Middle Atlantic Bight: terrestrial inputs and photooxidation. Limnology and Oceanography 42 (4), 674–686.

Walsh, J.J., Steidinger, K.A., 2001. Saharan dust and Florida red tides: the cyanophyte connection. Journal of Geophysical Research, Oceans 106 (C6), 11597–11612.

Walsh, J.J., Dieterle, D.A., Meyers, M.B., Müller-Karger, F.E., 1989. Nitrogen exchange at the continental margin: a numerical study of the Gulf of Mexico. Progress in Oceanography 23, 245–301.

Walsh, J., Dieterle, D., Muller-Karger, F., Bohrer, R., Bissett, W., Varela, R., Aparicio, R., Diaz, R., Thunell, R., Taylor, G., Scranton, M., Fanning, K., Peltzer, E., 1999. Simulation of carbon–nitrogen cycling during spring upwelling in the Cariaco Basin. Journal of Geophysical Research 104 (C4), 7807–7825.

Walsh, J.J., Penta, B., Dieterle, D.A., Bissett, W.P., 2001. Predictive ecological modeling of harmful algal blooms. Human and Ecological Risk Assessment 7, 1369–1383.

Walsh, J., Haddad, K., Dieterle, D., Weisberg, R., Li, Z., Yang, H., Muller-Karger, F., Heil, C., Bissett, W., 2002. A numerical analysis of landfall of the 1979 red tide of Karenia brevis along the West Coast of Florida. Continental Shelf Research 22, 15–38.

Walsh, J.J., Weisberg, R.H., Dieterle, D.A., He, R., Darrow, B.P., Jolliff, J.K., Lester, K., Vargo, G., Kirkpatrick, G.J., Fanning, K.A., Sutton, T.T., Jochens, A., Biggs, D., Nababan, B., Hu, C., Muller-Karger, F.E., 2003. The phytoplankton response to intrusion of slope water on the West Florida shelf: models and observations. Journal of Geophysical Research 108 (C6), 3190–3213.

Williams, P.M., Druffel, E.R.M., 1987. Radiocarbon in dissolved organic matter in the central North Pacific Ocean. Nature 330, 246–248.

Wroblewski, J.S., 1977. A model of phytoplankton plume formation during variable Oregon upwelling. Journal of Marine Research 35 (2), 357–394.

Yoder, J.A., Schollaert, S.E., O'Reilly, J.E., 2002. Climatological phytoplankton chlorophyll and sea surface temperature patterns in continental shelf and slope waters off the northeast U.S. coast. Limnology and Oceanography 47 (3), 672–682.